ROTATING TWO LEG BOSE HUBBARD LADDER

A THESIS

SUBMITTED TO THE DEPARTMENT OF PHYSICS

AND THE INSTITUTE OF ENGINEERING AND SCIENCE

OF BILKENT UNIVERSITY

IN PARTIAL FULFILLMENT OF THE REQUIREMENTS

FOR THE DEGREE OF

MASTER OF SCIENCE

By

Ahmet Keleş

August, 2009

I certify that I have read this thesis and that in my opinion it is fully adequate, in scope and in quality, as a thesis for the degree of Master of Science.

Assoc. Prof. Dr. M. Özgür Oktel (Supervisor)

I certify that I have read this thesis and that in my opinion it is fully adequate, in scope and in quality, as a thesis for the degree of Master of Science.

Prof. Dr. Cemal Yalabık

I certify that I have read this thesis and that in my opinion it is fully adequate, in scope and in quality, as a thesis for the degree of Master of Science.

Assoc. Prof. Dr. Azer Kerimov

Approved for the Institute of Engineering and Science:

Prof. Dr. Mehmet B. Baray
Director of the Institute Engineering and Science

ABSTRACT

ROTATING TWO LEG BOSE HUBBARD LADDER

Ahmet Keleş
M.S. in Physics
Supervisor: Assoc. Prof. Dr. M. Özgür Oktel
August, 2009

We analyze two leg Bose Hubbard model under uniform magnetic field within various methods. Before studying the model, we discuss the background on rotating Bose Einstein condensates, Bose Hubbard model and superfluid Mott insulator transition. We give a general overview of Density Matrix Renormalization Group (DMRG) theory and show some of the applications. Introducing two leg system Hamiltonian, we solve the single particle problem and find distinct structures above and belove a critical magnetic field $\alpha_c = 0.21\pi$. Above this value of the field, it is found that system has travelling wave solutions. To see the effects of interactions, we use Gross Pitaevskii approximation. Spectrum of the system below the critical field and the change of α_c with the interaction strength are obtained for small interactions, i.e $Un/t < 1$. To specify Mott insulator boundary, variational mean field theory and strong coupling perturbation (SCP) theories are used. The travelling wave solutions found in single particle spectrum above α_c is found to be persistent in mean field description. On the other hand, comparing with the strong coupling expansion results, it has been found that the mean field theory gives poor results, because of the one dimensional structure of the system. The change of the tip of the lobe where BKT transition takes place is found as a function of magnetic field by SCP. Finally we use DMRG to obtain the exact shape of the phase diagram. It is found that second order strong coupling perturbation theory gives very good results. System is found to display reenterant phase to Mott insulator. Looking at the infinite onsite interaction limit via DMRG, the critical value of the magnetic field is found to be exactly equal to the single particle solution. We have calculated the particle-hole gap for various fillings and different magnetic fields and found Fractional Quantum Hall like behaviors.

Keywords: Bose-Hubbard Model, Superfluid-Mott Insulator Transition, Renormalization, Strongly Correlated Systems.

ÖZET

DÖNEN İKİLİ BOSE HUBBARD MERDİVENİ

Ahmet Keleş
Fizik, Yüksek Lisans
Tez Yöneticisi: Yard. Doç. Dr. M. Özgür Oktel
Ağustos, 2009

Düzgün manyetik alan altındaki iki bacaklı Bose Hubbard modeli farklı yöntemlerle analiz edildi. Bu model çalışılmadan önce, dönen Bose Einstein yoğuşuklarının, Bose Hubbard modelinin ve süperakışkan Mott yalıtkanı geçişinin arka planı tartışıldı. Yoğunluk Matrisi Renormalizasyon Grubu (YMRG) teorisi genel olarak anlatıldı ve bazı uygulamaları gösterildi. İki bacaklı sistemin Hamiltonyeni verildikten sonra, tek parçacık problemi çözüldü ve kritik bir manyetik alanının $\alpha_c = 0.21\pi$ altında ve üstünde birbirinden farklı yapılanmalar bulundu. Kritik manyetik alanın bu değerinin üzerinde, hareketli dalga çözümleri bulundu. Etkileşimlerin etkilerini görmek için, Gross Pitaevskii yaklaşımı kullanıldı. Sistemin kritik manyetik alan altındaki spektrumu ve α_c'nin etkileşim kuvvetiyle değişimi zayıf etkileşimler için, $Un/t < 1$, bulundu. Mott yalıtkanı sınırının belirlenmesi amacıyla ortalama alan ve güçlü bağlaşım perturbasyonu (GBP) teorileri kullanıldı. Tek parçacık spektrumunda bulunan, kritik manyetik alan üzerindeki hareketli dalga çözümlerinin ortalama alan teorisinde de kullanılması gerektiği görüldü. Diğer yandan, güçlü bağlaşım teorisiyle karşılaştırma sonuçunda, sistemin bir boyutlu yapısından da dolayı, ortalama alan teorisinin kötü sonuç verdiği bulundu. BKT geçişinin olduğu, Mott yalıtkanı alanlarının tam uç noktasının manyetik alan ile değişimi GBP ile bulundu. Son olarak, YMRG kullanılarak faz diyagramının kesin şekli elde edildi. Bu sonuçlarla ikinci dereceye kadar yapılan GBP sonuçlarının çok iyi olduğu görüldü. Sistemin Mott yalıtkanı fazına geri-giriş gösterdiği görüldü. Sonsuz site-içi etkileşimine YMRG ile bakılarak, manyetik alanın kritik değerinin tek parçacık çözümüne tam alarak eşit olduğu görüldü. Parçacık-boşluk enerji aralığı değişik dolum oranlarınında ve manyetik alanlarda hesaplandı ve Kesirli Kuantum Hall Etkisine benzeyen davranışlar gözlemlendi.

Anahtar sözcükler: Bose-Hubbard Modeli, Süperakışkan-Mott Yalıtkanı Geçişi, Renormalizasyon, Güçlü Bağlaşık Sistemler.

Contents

List of Figures

List of Tables

Chapter 1

Introduction

Achievement of Bose Einstein condensation (BEC) has made a revolution in the development of many body physics in both theoretical and experimental studies. Being born at the intersection of disciples like Quantum Optics, Condensed Matter Physics and Atomic Physics, BEC has grown out to be a totally new branch of physics. In this chapter, we are going to give a short introduction to the basic concepts, generally discussing the theoretical foundation of the phenomena and consider the effect of fast rotation.

1.1 BEC: General Overview

Wave function describing a collection of identical quantum particles is either symmetric or anti-symmetric under the exchange of two particles. This exchange symmetry comes from the indistinguishability of the particles and separates the nature into two different class of statistics. Bosons are identified by the integer total spin and obey the Bose Einstein distribution, whereas fermions have half integer spin and obey Fermi Dirac distribution. For fermions, there is an exchange force coming from the antisymmetry of the wavefunction. It prevents two particles from occupying the same energy level and called Pauli exclusion principle. On the other hand, there is no such constraint for bosons so that

infinitely many particles can be placed in the same energy eigenstate. Though fermions have interesting physics, we are mainly interested in bosons, particularly the macroscopic occupation of a single eigenstate in this thesis.

For a collection of bosonic atoms, having energy eigenstates E_i, the occupation number of each state is given by the Bose Einstein statistics

$$\langle n_i \rangle = \frac{1}{e^{\beta(E_i-\mu)} - 1} \tag{1.1}$$

where $\beta = 1/kT$ is the inverse temperature, k is Boltzmann constant and μ is the chemical potential. In the limit of low temperature ($T \to 0$ or $\beta \to \infty$) the exponential term diverges and the occupation number of each state goes to zero so that one of the states must be filled separately. It is a standart textbook exercise to make this argument more quantitative. Defining the external potential to provide the exact energy spectrum and the dimensionality, a critical temperature where particles settle down to the ground state can be found [1, 2]. Another simple approach to see the peculiarity about absolute zero can be obtained by comparing the kinetic energies of particles ($p^2/2m$) with the thermal energy (kT) via the help of De Broglie relation $\lambda = h/p$ (h is Planck's constant). One can obtain a relation of the form $\lambda \propto \sqrt{h^2/2mkT}$. Thus as the temperature of the system goes to zero, particles will have a giant matter wave structure [3, 4].

BEC is defined as the macroscopic occupation of one of the single particle energy levels. Let $\Psi_s(x_1, x_2, \ldots, x_N)$ be set of many-body wavefunctions of a collection of N particles which is symmetric under the exchange of two particles, with weights w_s. Single particle reduced density matrix is defined as[5]

$$\rho_1(x, y) = N \sum_s w_s \int dx_2 dx_3 \ldots dx_N \Psi_s^*(x, x_2, \ldots, x_N) \Psi_s(y, x_2, \ldots, x_N) \tag{1.2}$$

where we have assumed one dimensional system for simplicity but this can be extended to three dimension and time dependence can be considered. From Eq.(1.2) it is seen that the density matrix $\rho_1(x, y)$ is Hermitian, thus it can be put into a diagonal form,

$$\rho_1(x, y) = \sum_i n_i \phi_i^*(x) \phi_i(y) \tag{1.3}$$

where ϕ is the complete set of orthogonal states. The coefficients in this expansion can be found by exploiting the orthogonality $\langle\phi_n|\phi_m\rangle = \delta_{nm}$ as

$$n_i = \int \phi^*(y)\rho_1(x,y)\phi(x)dxdy. \tag{1.4}$$

Formal definition of BEC: If one of the eigenvalues n_0 in Eq.(1.3) is order of total number of particles so that, sum in Eq.(1.3) has to be done by separating the dominant term[6]; like $\rho_1(x,y) = n_0\phi_0^*(x)\phi_0(y) + \sum_{i\neq 0} n_i\phi_i^*(x)\phi_i(y)$, then the system is said to be Bose condensed[5, 6, 7]. Accumulation of particles on one of the single particle eigenstates enables a simple form for the many body wave function. Condensate wave function can be written as

$$\Phi(\mathbf{r}) = \sqrt{N}\psi_0(\mathbf{r}) \tag{1.5}$$

where it is normalized to the total number of particles. In this expression, $\psi_0(\mathbf{r})$ is a complex valued function and called order parameter. One can safely write this function of the form $\psi_0(\mathbf{r}) = |\psi_0(\mathbf{r})|e^{i\theta}$, where θ is a function of $\mathbf{r}$.

To extend the discussion further, it is necessary to introduce system Hamiltonian. Hamiltonian for a system of N particles interacting via the two body interatomic potential $V(\mathbf{r}-\mathbf{r}')$ is given in second quantization

$$H = \int d\mathbf{r}\hat{\Psi}^\dagger(\mathbf{r})H_0\hat{\Psi}(\mathbf{r}) + \frac{1}{2}\int d\mathbf{r}d\mathbf{r}'\hat{\Psi}^\dagger(\mathbf{r})\hat{\Psi}^\dagger(\mathbf{r}')V(\mathbf{r}-\mathbf{r}')\hat{\Psi}(\mathbf{r})\hat{\Psi}(\mathbf{r}') \tag{1.6}$$

where $\hat{\Psi}(\mathbf{r})$ and $\hat{\Psi}^\dagger(\mathbf{r})$ are bosonic field operators that create and annihilate a particle at position $\mathbf{r}$ which satisfy the commutation $[\hat{\Psi}(\mathbf{r}), \hat{\Psi}^\dagger(\mathbf{r})] = \delta(\mathbf{r}-\mathbf{r}')$, all other commutators being zero, and H_0 is the noninteracting part of the Hamiltonian given by $H_0 = \hbar^2\nabla^2/2m + V_{ext}(\mathbf{r})$. The term $V_{ext}(\mathbf{r})$ in H_0 is external potential which is generally a harmonic oscillator potential. For a dilute gas at low temperature the interaction comes from two body collisions and given by[1, 5, 8]

$$V(\mathbf{r}-\mathbf{r}') = \frac{4\pi\hbar^2 a}{m}\delta(\mathbf{r}-\mathbf{r}') \tag{1.7}$$

where a is the s-wave scattering length.

1.1.1 Gross Pitaevskii Equation

A first strike at Eq.(1.6) is the exploitation of the mean field approximation. This is essentially nothing but the replacement of the field operator with a classical field such as Eq.(1.5). To obtain the equation of motion, one uses Heisenberg equation $i\hbar\partial\hat{\Psi}/\partial t = [\hat{\Psi}, \hat{H}]$ which gives

$$i\hbar\frac{\partial\Phi(\mathbf{r},t)}{\partial t} = -\frac{\hbar^2\nabla^2}{2m}\Phi(\mathbf{r},t) + V_{ext}(\mathbf{r})\Phi(\mathbf{r},t) + \frac{4\pi\hbar^2 a}{m}|\Phi(\mathbf{r},t)|^2\Phi(\mathbf{r},t). \quad (1.8)$$

This equation is called Gross-Pitaevskii equation. As long as the diluteness condition $na^3 \gg 1$ (n is density of the condensate and a is s-wave scattering length) is satisfied, this equation describes the condensate precisely in zero temperature limit[1, 8]. Assuming a time dependence of the form $\Phi(\mathbf{r},t) = \Phi(\mathbf{r})e^{-i\mu t/\hbar}$ in the wavefunction, time independent Gross-Pitaevskii equation can be obtained as

$$\left[-\frac{\hbar^2\nabla^2}{2m} + V_{ext}(\mathbf{r}) + g|\Phi(\mathbf{r})|^2\right]\Phi(\mathbf{r}) = \mu\Phi(\mathbf{r}) \quad (1.9)$$

where μ is the chemical potential and $g = 4\pi\hbar^2 a/m$. Eq.(1.9) is a nonlinear Schrödinger equation and exact solution is not always possible. There are several approaches for the approximate solution that will be mentioned briefly.

The first approach is variational, which is sometimes called ideal gas approximation. Having a solution to the non-interacting part of the Hamiltonian, a variational wavefunction can be defined that will minimize the energy. For an example, if the external potential is a harmonic oscillator potential, than the non-interacting part of the Hamiltonian will have a gaussian wave function in the ground state. Thus, defining a parameter dependent gaussian function that is properly normalized, one can obtain an upper limit for the energy. This method is proved to be very accurate to describe both the ground state properties and the collective excitations of Bose Einstein condensates.

Second approach is called Thomas-Fermi approximation. For sufficiently large number of atoms, the kinetic energy is much less than the interaction and potential energies. Thus one can ignore the kinetic energy term and solve the remaining algebraic equation for the chemical potential. Other quantities such as the total energy and the radius of the condensate can be obtained with this method.

Literature on Gross Pitaevskii equation is pretty diverse and we have not mentioned most of the important methods like numerical solutions or soliton solutions. Gross Pitaevskii theory is one of the very strong approaches for the analytical treatment of Bose Einstein condensates and a detailed analysis can be obtained from the references[1, 8]. A higher order approximation to Gross Pitaevskii theory is the so called Bogoliubov theory. Looking at small perturbations around the equilibrium wave function, one can consider the following[9]

$$\hat{\Psi} = \Phi + ue^{iwt} + ve^{-iwt} \tag{1.10}$$

and the excitation spectrum at higher order can be obtained.

1.2 Superfluidity and Rotating Condensates

Superfluidity was discovered by Kamerlingh Onnes with the experiments on He at low temperatures. Helium 4 is a superfluid that shows unusual properties below a specific temperature called lambda point, it has zero viscosity that diminishes the friction between the liquid and the container, zero entropy and infinite heat conductivity. These properties cause the liquid to display extraordinary properties. For example, superfluid helium can pass through very thin capillaries that it cannot pass above the lambda point. Another example is that the superfluid He can flow up through a tube plunged into it, which is called fountain effect. Among these surprises, the effect of rotation on superfluids is in particular interest of this thesis. If the container is rotated up to some particular angular velocity, superfluid does not rotate but stands still, whereas a classical fluid is expected to rotate. An interesting observation is the following. Assume that the container is rotated while the temperature is above the lambda point of Helium. Since temperature is not low enough, the fluid is classical and will rotate with the container. If the temperature is lowered below the transition temperature while it is still in rotation, the fluid will go on rotation to conserve the angular momentum. However, if the container is stopped, the superfluid will keep rotating without any change, indefinitely[7].

These unusual properties are later explained to be quantum mechanical by

Landau with his theory of quasiparticle excitations in liquid Helium[10]. The superfluidity of liquid helium comes from the partial Bose Einstein condensation that has taken place below lambda point. Though fraction of condensation (about %10) is pretty low, Bogoliubov approximation outlined in the previous section successfully describes its behavior[11].

We can figure out the effect of rotation on Bose Einstein condensates by using the condensate wave function. The order parameter defined in Eq.(1.5) is used to find particle current density

$$\mathbf{J} = \frac{\hbar}{2mi}\left[\psi_0^*\nabla\psi_0 - \psi_0\nabla\psi_0^*\right] \tag{1.11}$$

which can be found as $J = \hbar n_0 \nabla\theta/m$ where $n_0 = |\psi_0|^2$ is the density. Using the relation $\mathbf{J} = n\mathbf{v}$ the superfluid velocity can be found as

$$\mathbf{v_s} = \frac{\hbar}{m}\nabla\theta. \tag{1.12}$$

It follows from Eq.(1.12) that a superfluid defined by this order parameter is irrotational $\nabla \times \mathbf{v_s} = 0$, because curl of a gradient is zero for any function. An important consequence of this irrotationality follows from the surface integration of curl of the velocity field, which is defined as the circulation. Circulation is defined as: $\kappa = \int_S \nabla \times \mathbf{v_s} \cdot \mathbf{n} dS$, where n is the unit vector normal to the surface. Using Stokes theorem it can be written as $\kappa = \oint_C d\mathbf{l} \cdot \mathbf{v_s} = \oint_C d\mathbf{l} \cdot \nabla\theta$. Considering the single-valuedness of the wave function, the following relation can be obtained;

$$\kappa = \frac{2\pi\hbar}{m} l \tag{1.13}$$

which is called quantization of the circulation and l is an integer. This identity is the basis of irrotationality of the superfluid. It requires the quantized circulation which gives rise to formation of quantized vorticity in rotating superfluids. For the example of superfluid helium, the liquid does not respond to rotations upon small angular momentum. Whenever the critical rotation frequency is reached, a sudden vortex formation appears that carries a quantized angular momentum and a quantized circulation as given above. As the rotation frequency increases, the number of vortices increases. In the limit of fast rotations, these vortices form a regular array called vortex lattice. The meaning of fast rotation will be precise

in the next section. Vortex and vortex lattice formations are experimentally achieved in both superfluid Helium and Bose Einstein condensates of alkali metal gases.

The theory of vorticity in superfluids has remarkable similarities between the vorticity in superconductors. The analogy of irrotationality in superconductivity is the absence of a magnetic field inside a superconductor . It gives rise to the so called Meissner Effect. The magnetic field inside a superconductor vanishes but increasing the strength of the magnetic field, singularities start to form that magnetic field can pass through. In the limit of strong magnetic field, these singularities start to form a regular lattice which is called Abrikosov vortex lattice.

1.3 Landau Levels and Quantum Hall Regime

For a rotating condensate under the harmonic oscillator potential, the single particle Hamiltonian H_0, defined in Eq.(1.6) can be written as

$$H_0 = \frac{\mathbf{p}^2}{2m} + \frac{1}{2}mw^2\mathbf{r}^2 - \Omega\mathbf{L}_z \tag{1.14}$$

in the rotating frame of reference. For simplicity we assume a two dimensional condensate, trapped in a two dimensional isotropic potential. This assumption could be made much more subtle by considering a three dimensional condensate strongly trapped along z direction, but we will not consider this here for simplicity. The angular momentum operator is $L_z = xp_y - yp_x$, Ω is the frequency of the rotation and x, p_x obey the commutation $[x, p_x] = i\hbar$ (similar for y components). The creation and annihilation operators are defined as

$$\begin{aligned} a_x &= \frac{1}{\sqrt{2\hbar}}(m\omega x + ip_x) \\ a_y &= \frac{1}{\sqrt{2\hbar}}(m\omega y + ip_y) \end{aligned} \tag{1.15}$$

Table 1.1: Landau level index and corresponding angular momentum index for a two dimensional rotating condensate with isotropic harmonic confinement along the plane. The degeneracy increases as the energy eigenvalue is increased.

N	M
0	0
1	1, -1
2	-2, 0, 2
3	-3, -1, 1, 3

which satisfy the commutations $[a_x, a_x^\dagger] = 1$ and $[a_y, a_y^\dagger] = 1$, all other commutators being zero. Thus, the Hamiltonian in Eq.(1.14) can be cast into the form,

$$\begin{aligned} \frac{H}{\hbar\omega} &= (a_x^\dagger a_x + a_y^\dagger a_y + 1) + i\frac{\Omega}{\omega}(a_x^\dagger a_y - a_x a_x^\dagger) \\ &= \begin{pmatrix} a_x^\dagger & a_y^\dagger \end{pmatrix} \begin{pmatrix} 1 & i\Omega/\omega \\ -i\Omega/\omega & 1 \end{pmatrix} \begin{pmatrix} a_x \\ a_y \end{pmatrix} + 1. \end{aligned} \tag{1.16}$$

Diagonalization of 2×2 matrix in Eq.(1.16) is simple which gives the eigenvalues $\lambda_{1,2} = 1 \pm \Omega/\omega$. Thus the energy eigenvalues of the Hamiltonian can be written as,

$$E_{n,m} = \hbar(\omega + \Omega)n + \hbar(\omega - \Omega)m + \hbar\omega \tag{1.17}$$

where n and m are integers for band indices. In this form it is easy to see that the index n gives the main separation between the energy levels and it is called Landau Level index. The case $n = 0$ is called the lowest Landau level (LLL). It is interesting to consider the case $\Omega \to \omega$ which is called the rapid rotation limit introduced in previous section. In this case dependence of the energy to m vanishes and each Landau level becomes highly degenerate. In this limit, the separation between the lowest Landau levels become exactly $2\hbar\omega$.

It is often convenient to separate the energy coming from angular momentum in Eq.(1.17). Energy can be written as $E_{n,m} = \hbar\omega + \hbar\omega(n + m) - \hbar\Omega(m - n)$ and new indices $N = n + m$, $M = m - n$ can be introduced. In this form, $E \sim \hbar\omega N - \hbar\Omega M$, where N in the index of the energy level and M is the angular momentum number. Three different regions can be identified along with this form of the eigenstates[9]: *i- Weak Rotation($\Omega \approx 0$)*: The energy levels

depend only on the index N and each state shown in Table.1.1 is degenerate within the allowed angular momentum quantum numbers. The degeneracy is splitted for small values of angular frequency. *ii- Moderate Rotation($\Omega > 0$)*: The degeneracies of the weak rotation is now removed because of the Coriolis force coming from the angular momentum. *iii- Fast Rotation($\Omega \approx \omega$)*: A degeneracy different from the weak rotation comes out and the separation of energy levels is $2\hbar\omega$. The amount of angular momentum imposed on the condensate is very large and the gas forms a uniform array of quantized vortices (vortex lattice) to carry this angular momentum. This regime is sometimes called meanfield quantum Hall regime.

To see the effect of Coriolis force, another approach[12, 13] is performed to the Hamiltonian in Eq.(1.14). It can be shown that the following form is equivalent to the Hamiltonian in Eq.(1.14)

$$H = \frac{(\mathbf{p} - \mathbf{A})^2}{2m} + \frac{1}{2}m(\omega^2 - \Omega^2)r^2 \tag{1.18}$$

where $\mathbf{A}$ is the vector potential $\mathbf{A} = m\Omega \times \mathbf{r}$. This form is identical to the Hamiltonian of a charged particle in a magnetic field. This shows that the rotation decreases the effect of the harmonic confinement. The strength of Coriolis force is limitted by the oscillator frequency. In the limit $\Omega \to \omega$, it cancels the harmonic confinement and the condensate flies apart.

It is an experimental challenge to put the condensate in the meanfield quantum Hall regime. In the current experiments, rotation frequency attained is 99% of the oscillator frequency[14]. The difficulty of rapid rotation comes from the upper limit set by the harmonic trap. There are, on the other hand, some works that propose to add a quadric potential to the harmonic trap which has been shown to indicate promising implications like a giant vortex formation or the entrance to the quantum Hall regime[15]. Another direction for the exploration of fast rotation limit is the use of optical lattices[16]. Considering a condensate loaded on a rotating optical lattice, it is possible to reach extremely fast rotation rates, which is experimentally achieved[17]. On the other hand, Description of rotating condensates in optical lattice is a difficult theoretical problem which we will mention extensively throughout the thesis.

1.4 Outline of the Thesis

In this thesis, we aim to study the nature of a fast rotating Bose Einstein condensate extensively. To provide fast rotation and get rid of the limit set by harmonic confinemet, we will focus on the condensates in optical lattices, which is described via the Bose Hubbard model. We will consider a toy model, two leg ladder, that mimics the characteristic properties of rotating Hubbard model. Though the model is in its simplest form, theoretical explanation of its physical properties is a challenge. For this reason, we have employed a bunch of theoretical and numerical methods for a reliable description.

The thesis is organized as follows: In Chapter 2 we will introduce the Bose Hubbard model and its basic property; the superfluid Mott insulator transition. We show its well established theoretical treatments within the mean field and the perturbation approximations. In Chapter 3, we will make a review of the density matrix renormalization group theory (DMRG) and show basic algorithms applied to one dimensional spin systems. Application of DMRG to Bose Hubbard model will be presented and the derivation of the superfluid Mott insulator transition will be shown. Finally, in the last part, Chapter 4, we will use all of these methods to analyze the rotating two leg Bose Hubbard ladder. It will be shown that system bears evidence of strongly correlated states.

Chapter 2

Bose Hubbard Model

Bose Hubbard Hamiltonian is a model that describes strongly correlated systems under periodic boundary conditions. This periodicity may come from the crystal structure or the periodic optical confinement of atoms in Bose Einstein condensates. It can be applied to a variety of bosonic or fermionic systems such as electrons in the semiconductor crystal, liquid helium, Josephson junction arrays and Bose Einstein condensates in optical lattices. Apart from the diversity of applications, the model is valid under both weakly and strongly interacting regions irrespective of the correlations included. Unfortunately an exact solution to this model is only possible under special circumstances, particularly for low dimensional systems like Bethe Ansatz solution. There are, however, very strong theoretical and numerical approaches valid in a wide range of system parameters. Some of them are the central point of this thesis and will be investigated in detail. In this chapter, this model will be introduced in the context of Bose Einstein condensates loaded onto optical lattices. Basic theoretical approaches will be presented like a mean field approximations and a perturbative expansion. An important property of the model, i.e superfluid to Mott insulator transition will be investigated extensively within those approximations.

2.1 Superfluid Mott Insulator Transition

Bose Hubbard model is analyzed by Fisher *et al.*[18] in a more general form and interplay between the superfluid and Mott insulator phases is introduced for the first time by using scaling theory to mainly study the criticality. Upon Jaksch *et al.*'s work[19] which shows the possibility of realization of Bose Hubbard model in Bose Einstein condensates on optical lattices, the model has taken a new direction towards the study of degenerate quantum gases. In [20], phase diagram is obtained within different meanfield approaches and failure of Bogoliubov approximation is shown which indicates the importance of interactions and correlations in optical lattices. The superfluid to Mott insulator transition is observed experimentally by Greiner *et al.*[21]. This work placed Bose Hubbard model in the center of researches on the strongly correlated systems[22, 23].

Bose Hubbard Hamiltonian is written as

$$H = -\sum_{\langle i,j \rangle} t_{ij} a_i^\dagger a_j + \frac{U}{2} \sum_i n_i(n_i - 1) - \mu \sum_i n_i \tag{2.1}$$

where t_{ij} is the hopping matrix element between the sites i and j, U is the onsite interaction energy and μ is the chemical potential that controls the total number of particles as a Lagrange multiplier. a_i and $a_i^\dagger$ are the creation and annihilation operators of site i and the number operator is $n_i = a_i^\dagger a_i$. Hopping is generally assumed to be between the nearest neighboring sites, thus it is shown by $\langle i, j \rangle$ in the sum. This Hamiltonian can be easily generalized to describe next nearest neighbor hopping, nearest neighbor interaction and disorder[18, 24].

For a fixed number of particles, two distinguished characters, which are completely different, can be identified in the above Hamiltonian. In the limit of zero hopping matrix t_{ij}, called the atomic limit, the system is dominated by the onsite interactions and total energy is minimized by uniform distribution of particles throughout the lattice. This provides a commensurate filling. Each site is independent of the others and has its own wave function. The many body wave

function of the system can be written as

$$|\Psi\rangle = \prod_{i}^{L} |n_0\rangle_i = \prod_{i}^{L} \frac{(a_i^\dagger)^{n_0}}{\sqrt{n_0!}} |vac\rangle \tag{2.2}$$

where $|vac\rangle$ stands for the vacuum state and L is the total number of lattice sites. There are exactly n_0 particles per site so that total number of particles is $N = Ln_0$. In the other limit, the onsite interactions are zero, the system has full translational symmetry and all of the particles form of a coherent wave that hope around the lattice. In this case any particle is said to be in the superposition of all sites. The many body wave function becomes

$$|\Psi\rangle = (|\Psi_{sp}\rangle)^N = \left(\frac{1}{\sqrt{L}} \sum_{i=1}^{L} a_i^\dagger |vac\rangle \right)^N \tag{2.3}$$

where $|\Psi_{sp}\rangle$ is the single particle wave function. The first limit is called the Mott insulator phase whereas the second one is the superfluid phase. For nonzero values of the hopping and onsite interaction, there is an interplay between the superfluid and Mott insulator states depending on the chemical potential μ.

Superfluid phase bears a coherence and has an order parameter related to long range order. Particle number fluctuations are as large as the average site occupation, that is $\langle n_0^2 \rangle - \langle n_0 \rangle^2 \approx n_0^2$. Particles are delocalized. As a consequence, the average number of particles on a site may not be integer; the system has incommensurate filling. There is no gap for particle hole excitations, $E(N \pm 1) = E(N)$ and the system is compressible (compressibility $\kappa = \partial N / \partial \mu \neq 0$). Mott insulator phase is completely incoherent and each site is almost independent of each other. Particle number fluctuations are zero, particles are localized to the sites. The average number of particles per site is integer and system has a commensurate filling. There exists a finite gap for particle hole excitations making the system incompressible.

Onset of superfluidity is determined by the competition between the hopping and the onsite interaction terms. In atomic (or strong coupling) limit, system is Mott insulator if there is integer number of particles equal at all sites. As the hopping strength is increased, localization of particles will be lost. Two different types of phase transitions are expected to appear as the hopping is increased. For

fixed number of particles transition will be driven by phase fluctuations. This transition is called Berezinskii, Kosterlitz and Thouless (BKT) transition. A different transition appears if the system is allowed to change total number of particles by making particle or hole excitations. This transition is seen in grand canonical ensemble and called generic phase transition. Thus a finite region is expected to exist for the Mott insulator phase in $\mu/U - t/U$ plane bounded by the generic phase transitions from above and below (because of particle hole symmetry) which ends up with the BKT transition point. The finite Mott regions, Mott lobes, are repeated for different values of average filling n_0. In the following we will give two different methods for the derivation of Mott lobes based on meanfield approximations and perturbative expansions. For simplicity we will assume a one dimensional system.

2.2 Mean Field Theory

Different sites in Hamiltonian in Eq.(2.1) are only connected through the hopping term. Without hopping, each site is independent so that the solution of the total Hamiltonian can be reduced to a simple form at a local site. In the meanfield approximation, effect of hopping from neighboring sites is considered only as a meanfield and equation is solved for a single site. This approximation decouples the terms like $a_i^\dagger a_j$. We give a complex amplitude to the expectation values of field operators a_i so that $\langle a_i \rangle = \psi$ and $\langle a_i^\dagger \rangle = \psi^*$. Thus $a_i^\dagger a_j$ can be written as

$$\begin{aligned} a_i^\dagger a_j &= \langle a_i^\dagger \rangle a_j + a_i^\dagger \langle a_j \rangle - \langle a_i \rangle \langle a_i^\dagger \rangle \\ &= \psi^* a_j + \psi a_i^\dagger - |\psi|^2 \end{aligned} \tag{2.4}$$

where ψ is order the parameter for the system. Here, a numerical meanfield approach[25] will be considered that decouples the Hamiltonian and solves it for the complex amplitudes self consistently.

Quantitative form of the superfluid-Mott insulator phase diagram of Bose

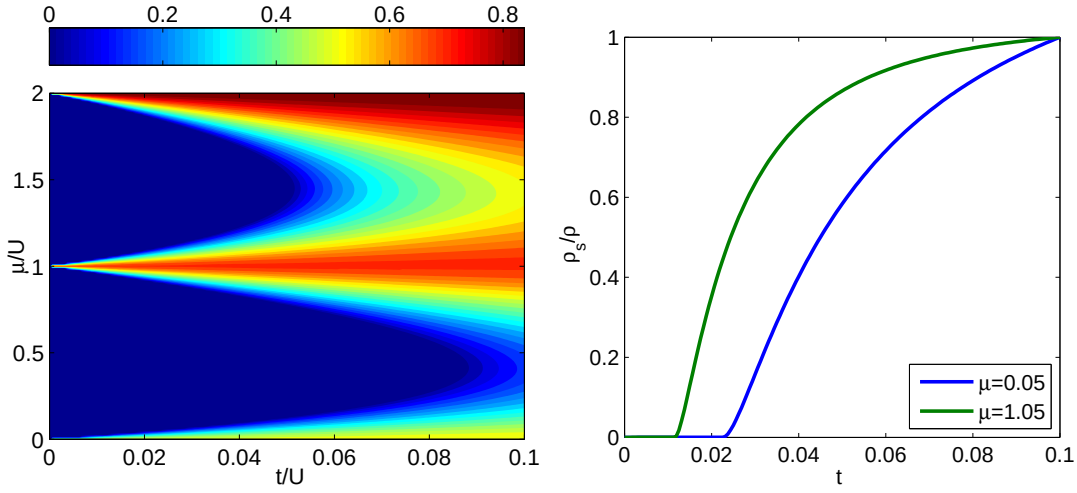

Figure 2.1: The order parameter calculated from self consistent meanfield approximation as a function of chemical potential μ and hopping t is shown on the left. The superfluid fraction as hopping in increased is shown on the right for two different chemical potentials.

Hubbard model is obtained by Sheshadri *et al.* by use of this numerical meanfield approximation. To show this method, we use one dimensional Bose Hubbard Hamiltonian. There are two nearest neighbors of each site under periodic boundary conditions. Thus making the decoupling shown in Eq.(2.4) an effective Hamiltonian valid for each site can be obtained as

$$H_i^{eff} = -t\left[2\psi a_i + 2\psi a_i^\dagger - 2|\psi|^2\right] + \frac{1}{2}n_i(n_i-1) - \mu n_i \tag{2.5}$$

where ψ is a constant for order parameter. Note that, in general ψ may be complex but we have taken it to be real for this specific case. The idea is the following: For some fixed value of t and μ, we find a maximum occupation number n_{max} for the Hamiltonian in Eq.(2.5) so that the ground state energy of the effective Hamiltonian H_i^{eff} is the same for its representations in the truncated basises n_{max} and $n_{max}+1$. Upon finding the maximum dimension of the truncated basis (n_{max}) we solve Eq.(2.5) to find its lowest eigenvalue and corresponding eigenvector. Let this eigenvector be $|G\rangle$, which is the ground state of effective Hamiltonian. We substitute the following for order parameter

$$\psi = \langle G|a_i^\dagger|G\rangle \tag{2.6}$$

and iterate this process until ψ converges. Repeating this route for each value of t and μ, corresponding scalar values of order parameters are obtained. The superfluid phase is identified with a nonzero order the parameter whereas order parameter of Mott insulator is zero.

In Fig.2.1, we have shown the results of our calculations for this one dimensional system. The order parameter is plotted with contours as a function of hopping and chemical potential. One can see that, there is a finite region where it is zero, shown by dark blue in the figure. This region is Mott insulator phase. As the parameters are varied, ψ start to take nonzero values indicating the superfluid Mott insulator transition. On the left panel of the same figure, we have shown the superfluid fraction for two different values of the chemical potential $\mu = 0.05, 1.05$ as a function of the hopping strength. We see that for very small hopping, there is no superfluid fraction in the system. Increasing the hopping until a critical value, around 0.01 for $\mu = 1.05$ and 0.02 for $\mu = 0.05$, system owns a small superfluid fraction. This transition is generic, i.e it is a density driven phase transition. On the other hand, BKT transition appearing at the tip of the first lobe is quantum phase driven transition and seen to be around $t_c = 0.09$.

2.3 Strong Coupling Expansion

Freericks *et al.* [26] introduced a different method to obtain the phase diagram. They considered particle and hole excitations as the energy levels of Bose Hubbard model and perturbatively calculated the corrections to the energy levels. This method is used to study pure[26] and disordered[27] systems and recently for extended Bose Hubbard model[28]. In this section, we will show the details of this strong coupling perturbation method for a one dimensional system.

Strong coupling expansion is a perturbative method that considers the hopping term as a small perturbation[26]. Hamiltonian is written as $H = H_0 + V$,

where

$$\begin{aligned} H_0 &= \frac{1}{2}\sum_i n_i(n_i-1) - \mu\sum_i n_i \\ V &= -\sum_{\langle i,j\rangle} t_{ij} a_i^\dagger a_j \end{aligned} \tag{2.7}$$

and U is taken to be one. Rayleigh-Schrödinger perturbation expression for the energy up to second order can be written in its well known form,

$$\begin{aligned} E_k &= E_k^{(0)} + E_k^{(1)} + E_k^{(2)} + \dots \\ &= E_k^{(0)} + \langle\Psi_k^{(0)}|V|\Psi_k^{(0)}\rangle + \sum_{i\neq k} \frac{|\langle\Psi_k^{(0)}|V|\Psi_i^{(0)}\rangle|^2}{E_k^0 - E_i^0} + \dots \end{aligned} \tag{2.8}$$

where k is the state label that the correction will be done and $|\Psi_k^{(0)}\rangle$ is the wave function of this state. In the case of degeneracy, matrix representation of the perturbation in the degenerate subspace is calculated and $|\Psi_k\rangle$ is chosen as the ground state of this matrix. Exclusion of the state k in the sum turns out to be exclusion of all states in the degenerate set, i.e $i \neq k$, for all $k \in D$, D is the degenerate set. In the following we will show the calculation of perturbation series up to second order for one dimensional Hubbard model to demonstare the method.

Mott insulator state is characterized by a finite nonzero gap as mentioned earlier. Gap is defined as the energy difference between two states; one with n_0 particles in each lattice site and the other with a defect (one extra particle or hole in one of the lattice sites). Let energies be shown by E_m, E_p and E_h for n_0 particles per site, one extra particle and one extra hole respectively. Thus $E_p - E_h$ and $E_m - E_h$ will be nonzero at Mott insulator state. The place where these gaps vanish will give the boundary of the Mott insulator state. In zeroth order, atomic limit, the particle and hole excitation gaps can be written as

$$\begin{aligned} E_p^{(0)} - E_m^{(0)} &= E(n_0+1) - E(n_0) = n_0 - \mu_p \\ E_m^{(0)} - E_h^{(0)} &= E(n_0) - E(n_0-1) = (n_0-1) - \mu_h \end{aligned} \tag{2.9}$$

where $E(n_0) = n_0(n_0-1)/2 - \mu n_0$ is the single site energy. It can be seen that, even in the atomic limit where hopping is not allowed, system can be in

the superfluid phase for $\mu = n_0$ or $\mu = n_0 - 1$ (at zero temperature). In the following the energies of Mott and defect (particle and hole) states are calculated perturbatively for nonzero hopping.

Mott State

In Mott state, all of the particle are localized and there are exactly n_0 perticles at each site. To the zeroth order, ground state of the system can be written as

$$|\Psi_M^{(0)}\rangle = \prod_{k=1}^{L} \frac{(a_k^\dagger)^{n_0}}{\sqrt{n_0!}}|vac\rangle \tag{2.10}$$

where L is the number of lattice sites. The first order correction can be calculated from Eq.(2.8) as $E_M^{(0)} = \langle\Psi_M^{(0)}|V|\Psi_M^{(0)}\rangle = 0$, because $\langle\Psi_M^{(0)}|a_i^\dagger a_j|\Psi_M^{(0)}\rangle$ will be zero for all $i \neq j$. The second order terms requires the calculation of matrix elements $\langle\Psi_M^{(0)}|V|\Psi_k^{(0)}\rangle$, where $|\Psi_k^{(0)}\rangle$ is the set of all eigenvectors except the Mott state. Explicit form of this term can be written as

$$\langle\Psi_M^{(0)}|V|\Psi_k^{(0)}\rangle = -\sum_{ij} t_{ij}\langle\Psi_M^{(0)}|a_i^\dagger a_j|\Psi_k^{(0)}\rangle. \tag{2.11}$$

The elements of the sum will be nonzero only for the eigenvectors of the form

$$|\Psi_k^{(0)}\rangle = \frac{a_i^\dagger a_j}{\sqrt{n_0(n_0+1)}}|\Psi_M^{(0)}\rangle$$

where it is written in normalized form and $i \neq j$ since otherwise it would be the Mott state wave function. Also, i and j have to be nearest neighbors. For a one dimensional model there are N such states. Matrix element for a particular such state is found from the above wave function as $\langle\Psi_M^{(0)}|V|\Psi_k^{(0)}\rangle = -t\sqrt{n_0(n_0+1)}$. Energy difference between this state and the Mott state can be calculated by considering that there are one extra particle and one extra hole in this state. Thus the energy difference can be found as $E_k^{(0)} - E_M^{(0)} = -1$. Using these calculations, the second order correction is found from Eq.(2.8). The energy of the Mott state up to second order is found as,

$$E_M = E_M^{(0)} - 2Nt^2 n_0(n_0+1) + O(t^3). \tag{2.12}$$

Defect States

Correction to the defect states will be calculated in a similar manner. However there is an important difference from the Mott state calculations: ground state of the defects are N-fold degenerate, where N is the number of lattice sites. Because an extra particle or hole can be placed N different places on the lattice each having the same energy. Thus, we will use degenerate perturbation theory for the first order correction. General normalized eigenvectors in this degenerate set can be written as

$$|\Psi^{(0)}_{P,i}\rangle = \frac{a_i^\dagger}{\sqrt{n_0+1}}|\Psi^{(0)}_M\rangle, \quad |\Psi^{(0)}_{H,i}\rangle = \frac{a_i}{\sqrt{n_0}}|\Psi^{(0)}_M\rangle \tag{2.13}$$

where P and H stand for particle and hole respectively and i runs from 1 to N.

Let us first consider the correction to the particle state. Construction of the matrix representation of the perturbation in this degenerate set will be done by using $V_{i'i} = \langle\Psi^{(0)}_{P,i'}|V|\Psi^{(0)}_{P,i}\rangle$, which gives

$$V_{i'i} = -(n_0+1)t_{i'i}. \tag{2.14}$$

Lowest eigenvalue of the hopping matrix can be calculated by Fourier transforming the hopping term, which will give 2 in one dimension. Thus first order correction to energy will be $E^{(1)}_P = -2t(n_0+1)$. Let the corresponding eigenvector of this matrix V be shown by $\vec{f}$. This will be used to find the correct form of the ground state wave function as,

$$|\tilde{\Psi}^{(0)}_P\rangle = \sum_i f_i \frac{a_i^\dagger}{\sqrt{n_0+1}}|\Psi^{(0)}_M\rangle. \tag{2.15}$$

Using this wavefunction in Eq.(2.8) the second order correction is found and the total energy up to second is

$$E_P = E^{(0)}_M + n_0 - \mu_p - 2t(n_0+1) - 2Nt^2n_0(n_0+1) + t^2n_0(5n_0+4) - 4t^2n_0(n_0+1). \tag{2.16}$$

Making the similar calculations for extra hole state, energy up to second order can be found as

$$E_H = E^{(0)}_M + \mu_h - (n_0-1) - 2tn_0 - 2Nt^2n_0(n_0+1) + t^2(n_0+1)(5n_0+1) - 4t^2n_0(n_0+1). \tag{2.17}$$

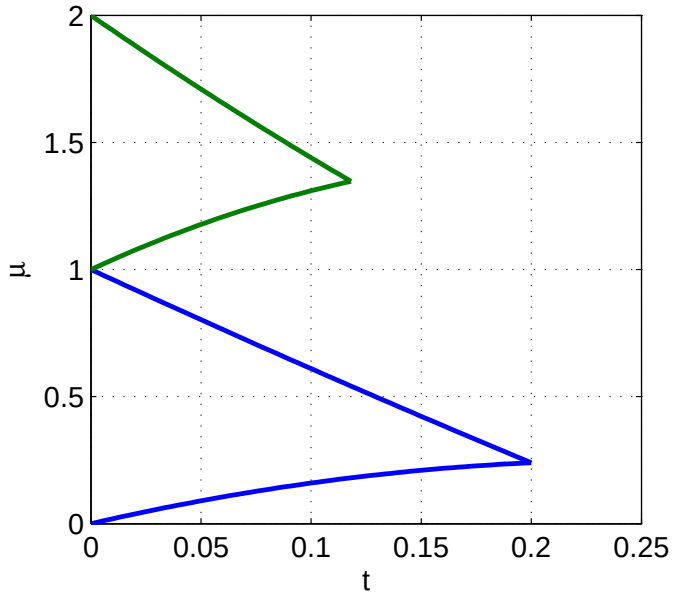

Figure 2.2: Phase diagram of one dimensional Bose Hubbard Model calculated from strong coupling perturbation up to second order.

Boundaries of the Mott insulator region will be found by solving $E_P - E_M = 0$ for μ_p, and $E_M - E_H = 0$ for μ_h. μ_p and μ_h give upper and lower boundaries respectively. They are found to be

$$\begin{aligned} \mu_p &= n_0 - 2t(n_0+1) + t^2 n_0^2 \\ \mu_h &= (n_0 - 1) + 2n_0 t - t^2(n_0+1)^2. \end{aligned} \tag{2.18}$$

In Fig.2.2, we plot the boundaries found in Eq.(2.18) for the first two lobes $n_0 = 1$ and $n_0 = 2$. The critical point that the BKT transition takes place is seen to be at $t_c = 0.2$. Comparison with the mean field calculation gives inconsistent results. However we have shown both methods to show the details of the methods. The decoupling approximation employed in the meanfield theory fails especially for low dimensional systems where correlations are more pronounced. On the other hand, strong coupling expansion is very strong for one dimensional systems. In the next chapter, we will show the exact shape of phase diagram by using density matrix renormalization group theory. One can see the power of the strong coupling expansion by looking at this section of thesis.

2.4 Rotation in Bose Hubbard Model

Inclusion of a rotation to Bose Hubbard model is done by Pierls substitution, which is based on the analogy between the rotation and the magnetic field presented in Chapter 1. For a two dimensional optical lattice rotating around an axis perpendicular to the plane, Hamiltonian in Bose Hubbard model can be written as

$$H = -t \sum_{\langle i,j \rangle} e^{iA_{ij}} a_i^\dagger a_j + \frac{U}{2} \sum_i n_i(n_i - 1) - \mu \sum_i n_i \tag{2.19}$$

where $\mathbf{A}$ is the vector potential that satisfies $\mathbf{B} = \nabla \times \mathbf{A}$. Single particle spectrum of this model was first considered by Hofstadter[29], in the context of electrons in magnetic field. The range of magnetic field he argued was so large that it did not get much attention by that time. However, the effective magnetic field in rotating Bose Hubbard model is quite successfull for creation of these strong fields.

The energy spectrum of Bose Hubbard model under magnetic field gives Hofstadter butterfly, which is strongly related to the Landau levels[30]. Thus, rotating optical lattices provides a possibility to realize the exotic quantum phases in the the fast rotation limit[31]. There has been a bunch of proposals and treatments for the realization and detection of these strongly correlated phases[32, 33, 34, 35, 36]. But these works are limited to exact diagonalization studies of a few number of particles on a few lattice sites which are far from thermodynamic limit. However they have promising results for the discovery of fractional quantum Hall states in the optical lattice setups. Recently, a composite fermion theory adapted to rotating Hubbard model is used to show the overlap of groundstate wavefunction with the Loughlin state[37]. Theoretical and numerical tools are quite limited for the exploration of rotating Hubbard model. The strongest approaches are meanfield theory and strong coupling expansion which are both applied to rotating model in [38] and [39] to find the Mott phase boundary. Motivated by these works, we will analyze a toy model, rotating two leg Hubbard ladder, within these methods in the following chapters. Apart from all, we will use density matrix renormalization group theory to study exact nature of this simple quasi-one dimensional system.

Chapter 3

Density Matrix Renormalization Group Theory

Study of strongly correlated systems is one of the most active research areas of both theoretical and experimental condensed matter physics. Bose Einstein condensates, Fermi gases, spin chains, superconducting curprates, Josephson junction arrays, cold atoms in optical lattices and even the quantum entanglement can be given as examples of strongly correlated systems. Models of these systems like Bose Hubbard model, Heisenberg spin Hamiltonian or t-J model contain the key properties that display rich physical phenomena such as Mott transition, spin gap, superconductivity etc. Yet, the solutions of these systems are difficult. Analytical treatments are quite inadequate for the observation of important transitions. For example, mean field theory does not include the effect of correlations whereas the perturbative approaches have limited range of validity due to the strength of correlations. This makes computer simulations indispensable tools for the exploration of strongly correlated systems.

On the other hand, numerical solution of those systems is not an easy job, either. Exponential growth of the total Hilbert space dimension with increasing lattice size makes it impossible to treat systems properly even for the strongest computers today. Consider, for example, spin-1/2 antiferromagnetic Heisenberg

chain, in which each individual site has a two dimensional Hilbert space. Hilbert space grows as 2^N with the number of lattice sites N which makes it very difficult to simulate above a dozen of lattice sites.

Density Matrix Renormalization Group Theory (DMRG), developed by S.R. White[40, 41, 42] as an extension of Wilson's numerical renormalization group method[43], is one of the strongest numerical approaches for the study of strongly correlated quantum lattice models in one dimension. It systematically reduces the dimension of the total Hilbert space by use of density matrices. Since its invention it has been applied to a variety of lattice systems[44]. It is regarded as giving the numerically exact solution but its main drawback is the absence of implementation to higher than one dimensional systems which is currently an active research area[45].

3.1 Exact Diagonalization

To introduce the mechanism of DMRG, the exact diagonalization methods will be mentioned briefly. In this method, one considers the full Hilbert space of the system as the direct products of the Hilbert spaces of the constituent subsystems and solves the resulting eigenvalue problem exactly. There is no approximation involved, thus this method gives exact solution for all parameter values up to machine precision.

Consider a lattice system, that has local sites each having a finite Hilbert space h_i with the dimension d_i. One can write the full Hilbert space of a two site system, for example, as $H_2 = h_1 \otimes h_2$ where $\otimes$ is the direct product or Kronecker product and the dimension of the total Hilbert space becomes $d_1 d_2 = d^2$. Similarly a three site system can be written as $H_3 = h_1 \otimes h_2 \otimes h_3$ where the dimension of total Hilbert space becomes $d_1 d_2 d_3 = d^3$. In general for an N site system, the full Hilbert space can be written as

$$H_N = h_1 \otimes h_2 \otimes \cdots \otimes h_N \tag{3.1}$$

with the dimension being $d_1 d_2 \ldots d_N = d^N$. It is seen that Hilbert space grows

exponentially with increasing the number of sites. This is the reason why exact diagonalization method is not applicable to all problems. It is difficult to figure out the properties of a system in the thermodynamic limit by use of exact diagonalization.

For the reduction of the matrices to be diagonalized, the symmetries of the system should be used. Conservation of the total angular momentum along z-direction in antiferromagnetic Heisenberg model or the total number of particles in Bose Hubbard model can be given as examples for the symmetries that can be used. Consider one dimensional Heisenberg spin model. The Hamiltonian of this model is

$$H = -J \sum_i S_i \cdot S_{i+1}. \tag{3.2}$$

For a simple system of 6 sites, Hilbert space dimension is $2^6 = 64$. On the other hand we know that the ground state of the system will be in $S^z_{total} = 0$ state. This reduces the dimension down to 20, which is much less than that of the total space. Symmetries to be used change from system to system but exploitation of them is crucial for all numerical methods. To do this, one needs to find a quantity that commutes with the Hamiltonian so that the Hamiltonian can be written in block diagonal form and matrices to be solved will be much smaller.

3.2 Density Matrix

Consider an arbitrary state ket $|\phi\rangle$. We define an operator like $P = |\phi\rangle\langle\phi|$, which is a projection operator on to the defined vector. What is the matrix representation of this operator in a given basis? The matrix elements of the operator can be written as $P_{ij} = \langle i|\phi\rangle\langle\phi|j\rangle$. Expanding the kets in a set of complete states as $|\phi\rangle = \sum_{i'} c_{i'}|i'\rangle$, one can arrive at the following simple form; $P_{ij} = c_i c_j^*$. For the case $i = j$ the interpretation of this expression is straightforward: it is the probability that the system can be in a specific state i. The case $i \neq j$, which will be clear soon, seems to be undefined from a quantum mechanical point of view. This can be made further complicated by slightly modifying the projection operator P as; $P = A|\phi_1\rangle\langle\phi_1| + B|\phi_2\rangle\langle\phi_2|$ where $|\phi_1\rangle$ and $|\phi_2\rangle$ are some arbitrary

state vectors, which may or may not be orthogonal to each other. Action of this operator is interpreted as the projection to two different states with some weights A and B. Expanding the kets in a complete basis, $|\phi_1\rangle = \sum_{i'} c_{i'}|i'\rangle$ and $|\phi_2\rangle = \sum_{i'} d_{i'}|i'\rangle$, one can find the matrix representation of this operator as $P_{ij} = Ac_i c_j^* + Bd_i d_j^*$. It is important for the case $i = j$ that other weighting factors A and B are introduced in the formalism, apart from the usual quantum mechanical probabilities $|c_i|^2$ and $|d_i|^2$.

Density matrix is the most general description for a quantum mechanical system[46]. Quantum mechanics is established on the solution of Schrödinger equation which results with a set of complete eigenstates. Once this is done, any state $|\Psi\rangle$, whether an eigenstate of the Hamiltonian or not, can be described by those complete set of vectors. Whenever some physical quantity S is concerned, expectation values can be found as $\langle\Psi|S|\Psi\rangle$. On the other hand, real systems cannot be described by this formalism since they are completely random ensembles[46]. A collection of silver atoms in an oven or a beam of unpolarized light can be given as the examples of completely random ensembles or "mixed ensembles" in the language of density matrix. For the example of silver atoms, %50 of the atoms are spin up and %50 of them is spin down. Once they pass from a Stern-Gerlach apparatus, they split into two diverging beams which are now "pure ensembles", in terms of the z-components of the spins alone.

In general, density operator can be defined as,

$$\rho = \sum_i w_i |\phi_i\rangle\langle\phi_i| \tag{3.3}$$

where w_i's are the percentages in the above example that are the statistical probabilities in an ensemble. Density matrix is the matrix representation of this operator in a basis, which can be obtained as above (in a more general way) by using $|\phi_i\rangle = \sum_k c_k^i |k\rangle$, which gives

$$\rho_{kk'} = \sum_i w_i c_k^i (c_{k'}^i)^*. \tag{3.4}$$

Notice that both quantum mechanical and statistical probabilities are combined in the formalism. This is the basic purpose of the density matrix. Note that

$Tr(\rho) = 1$ and it can be shown that the expectation value of any operator A can be obtained as $\langle A\rangle = Tr(\rho A)$. By using maximization of Neumann entropy defined as $S = -Tr(\rho \ln \rho)$, it can also be shown that the weighting factors w_i are $e^{-\beta E_i}$ so that the form of the density matrix is $\rho = e^{-\beta H}/Z$, where Z is the partition function[2]. In the limit of low temperatures which means $\beta \to \infty$, only the ground state's weight becomes unity and all others zero. This is essentially a pure state as explained above. Thus at low temperature limit, density matrix is defined to be

$$\rho = |\Psi^0\rangle\langle\Psi^0| \tag{3.5}$$

3.2.1 Reduced Density Matrix

Physical systems are in general composite systems. System and heat bath or environment in statistical mechanics, two particles entangled in a Bell state can be given as specific examples for our purpose. Quantum mechanics treats a part of those composite systems independently and solves them as if the other part does not exits. Or, the solution is done for the whole composite system so that constituent parts lose their identity. Another very important concept related to the density matrix is the concept of reduced density matrix [47], which remedies this inconvenience. Consider a system composed of two parts as shown in Fig.3.1. Let the state vectors be $|i\rangle$ and $|j\rangle$ of each part A and B, respectively. Then the most general state of the total system can be written as

$$|\Psi\rangle = \sum_{ij} \Psi_{ij}|i\rangle|j\rangle \tag{3.6}$$

where Ψ_{ij} is the expansion coefficient. Assume we have an operator that acts only one part of the system and does nothing to the other part. Then what is the expectation value of this operator in state $|\Psi\rangle$? Let this operator be S^A, where

superscript A tells that it only acts on subsystem A. It can be evaluated as

$$\begin{aligned}\langle\Psi|S^A|\Psi\rangle &= \sum_{ij}\sum_{i'j'}\Psi_{ij}\Psi^*_{i'j'}\langle j'|j\rangle\langle i'|S^A|i\rangle \\ &= \sum_{iji'}\Psi_{ij}\Psi^*_{i'j}\langle i'|S^A|i\rangle \\ &= \sum_{ii'}S^A_{ii'}\left[\sum_j\Psi_{ij}\Psi^*_{i'j}\right]\end{aligned} \tag{3.7}$$

where the term in the parantesis is defined to be the reduced density matrix. It can be shown that it is equal to $\rho = Tr_B(|\Psi\rangle\langle\Psi|)$, where $Tr_B(\dots)$ means that the trace is taken over the states of the system B alone. Thus, the expectation value of the operator is $\langle S^A\rangle = Tr(\rho^A S^A)$. We can write the reduced density matrices of the subsystems A and B as

$$\begin{aligned}\rho^A_{ii'} &= Tr_B(|\Psi\rangle\langle\Psi|) = \sum_j\Psi_{ij}\Psi^*_{i'j} \\ \rho^B_{jj'} &= Tr_A(|\Psi\rangle\langle\Psi|) = \sum_i\Psi_{ij}\Psi^*_{ij'}.\end{aligned} \tag{3.8}$$

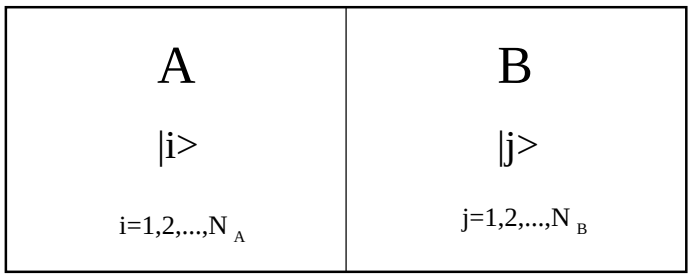

Figure 3.1: Schematic representation of a system composed of two parts A and B. $|i\rangle$ and $|j\rangle$ are the complete sets of states that span each subsystem.

3.2.2 Density Matrix Truncation

Assume that two systems A and B are in contact and correlated so that it is not possible to write a separable solution for the energy eigenstates. Let there be N_A

states in the system A and N_B states in B and let us label those states by $|i\rangle$ and $|j\rangle$, respectively, as shown in Fig.3.1. Then, the most general state of the total system A and B can be written in terms of complete set of states $|i\rangle$ and $|j\rangle$ as

$$|\Psi\rangle = \sum_{i=1}^{N_A}\sum_{j=1}^{N_B}\Psi_{ij}|i\rangle|j\rangle. \tag{3.9}$$

We want to take M most relevant states from the N_A states in A so that $N_A - M$ states will be swept out[44, 48]. We can write those M states of the form $|\alpha\rangle = \sum_{i=1}^{N_A} u_{\alpha i}|i\rangle$ where $\alpha = 1, ..., M$ and the expansion coefficients $u_{\alpha i}$ are to be determined later. We want to choose the most important states of the system A where 'important' refers to the minimization of the norm, $|||\Psi\rangle - |\tilde{\Psi}\rangle||$ for

$$|\tilde{\Psi}\rangle = \sum_{\alpha=1}^{M}\sum_{j=1}^{N_B} a_{\alpha j}|\alpha\rangle|j\rangle. \tag{3.10}$$

Assuming real coefficients in the expansions for simplicity, we have

$$|||\Psi\rangle - |\tilde{\Psi}\rangle||^2 = 1 - 2\sum_{ij\alpha}\Psi_{ij}a_{\alpha j}u_{\alpha i} + \sum_{\alpha j}a_{\alpha j}^2. \tag{3.11}$$

Taking the derivative of the above norm with respect to the coefficients $a_{\alpha j}$ and equating to zero, one finds that $a_{\alpha j} = \sum_i \Psi_{ij}u_{\alpha i}$. Inserting this expression into Eq.(3.11), one arrives at

$$\begin{aligned} |||\Psi\rangle - |\tilde{\Psi}\rangle||^2 &= 1 - \sum_{ij\alpha i'}\Psi_{ij}\Psi_{i'j}u_{\alpha i}u_{\alpha i'} \\ &= 1 - \sum_{ii'\alpha}u_{\alpha i}\rho_{ii'}u_{\alpha i'} \\ &= 1 - \sum_{\alpha}\langle\alpha|\rho|\alpha\rangle \end{aligned} \tag{3.12}$$

where ρ is the density matrix of the form $\rho_{ii'} = \sum_j \Psi_{ij}\Psi_{i'j}$. For Eq.(3.12) to be minimum $|\alpha\rangle$'s must be eigenvectors corresponding to the largest eigenvalues of the density matrix $\hat{\rho}$, by Rayleigh-Ritz principle[44].

Thus, we arrive at the following conclusion. Once we have a very large Hilbert space, we can systematically reduce the dimension by looking at the density matrix eigenvalues. In DMRG, system is enlarged to a higher dimension by adding a site to it and then reduced back to the beginning with the density matrix projections. This will be explained in detail in the next section.

3.3 DMRG Algorithms

DMRG is a renormalization group method that uses density matrices for systematic reduction of extra degrees of freedom[40]. In the standart block renormalization group, developed by Wilson[43], system size is doubled and states that has the lowest energies are discarded at each iteration, beginning from a single site. It is found that this method was unable to describe interacting systems properly. For example, it had failed for the description of a single particle in infinite well potential. White and Noach soon noticed that it was the boundary conditions that has to be taken care of. They fixed the failures of the method by defining different boundary conditions[49] which was soon generalized in the density matrix renormalization group method.

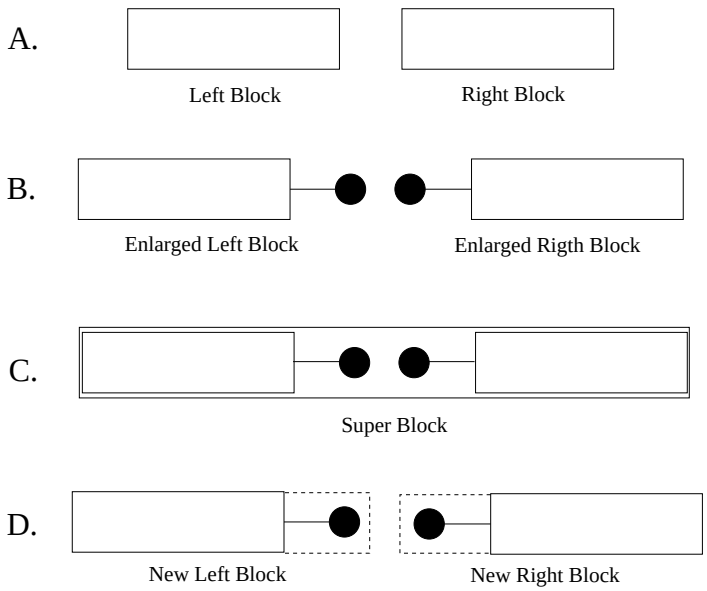

Figure 3.2: Infinite system algorithm.

We have mentioned how to enumerate the states of a system, according to their significance, in the previous section. Thus we need to make such a construction that, it must be composed of two parts, which might be called as system and environment, respectively. In the language of DMRG this distinction is named by system block and environment block. In literature, blocks are named by left

block for the system and right block for the environment, because of the one dimensional structure of the models. Determination of the system and environment blocks is different in two different DMRG algorithms; infinite system and finite system algorithms. In the infinite system algorithm, system size is increased until convergence is obtained whereas in the finite system algorithm system size is fixed but the the convergence is obtained by so called sweeps which will be discussed later. To obtain a high numerical accuracy, infinite system algorithm is insufficient and one needs to perform the finite system algorithm[40, 41].

3.3.1 Infinite System Algorithm

In the infinite system algorithm, both left and right blocks are enlarged at each step, beginning from a single site, until the convergence is obtained. This process is illustrated in Fig.3.2. In the beginning, left and right blocks are represented by M-by-M matrices. Let us show left and right blocks by $B_L(k, M)$ and $B_R(k, M)$, respectively. In this notation k stands for the number of sites in the block and M is the dimension of the block. Similarly we represent a single site with $s(D)$, where D is the dimension of the site. Initially, we have right and left blocks as shown in Fig.3.2A. Now, we enlarge these blocks by adding sites as shown in Fig.2B. We have the left enlarged block $B_L(k, M) \otimes s(D)$ and the right enlarged block $s(D) \otimes B_R(k, M)$. The size of the matrices of the enlarged blocks increased to $MD \times MD$. At this step it is important to write the Hamiltonian and other relevant operators in the basis of an operator that commutes with the Hamiltonian. This provides a block diagonal form for the Hamiltonian. The next step is the formation of superblock Hamiltonian $[B_L(k, M) \otimes s(D)] \otimes [s(D) \otimes B_R(k, M)]$ which is shown if Fig.3.2C. This Hamiltonian is represented by $(M \times D)^2$-by-$(M \times D)^2$ matrix which is the largest matrix size that will be used. Thus it is crucial to employ symmetries in the formation of the superblock Hamiltonian. Then, the superblock Hamiltonian is diagonalized to find the lowest energy eigenstate with a sparse matrix diagonalization routine and the reduced density matrices are formed from Eq.(3.8). After that eigenvalues and eigenvectors of the density

matrix are found with a dense matrix diagonalization routine and then the eigenvectors corresponding to the lowest M eigenvalues are used for the formation of the projection matrices O_L and O_R as;

$$\begin{aligned} O_L &= (\vec{v}_1 \vec{v}_2 \dots \vec{v}_M) \\ O_R &= (\vec{u}_1 \vec{u}_2 \dots \vec{u}_M) \end{aligned} \tag{3.13}$$

where v_i's and u_i's are the eigenvectors of the left and right block density matrices corresponding to M largest eigenvalues. O_L and O_R are $MD \times M$ matrices. Using these matices, enlarged left and right block can be reduced to the dimension at the beginning by using;

$$\begin{aligned} B_L(k+1, M) &\rightarrow O_L^\dagger \left[B_L(k, M) \otimes s(D) \right] O_L \\ B_R(k+1, M) &\rightarrow O_R^\dagger \left[s(D) \otimes B_L(k, M) \right] O_R. \end{aligned} \tag{3.14}$$

This process is shown is Fig.3.2D. After this step, left and right blocks are updated and will be used as new blocks for the next iteration. After one iteration, the number of sites in a block is increased from k to $k+1$ which shows the linear growth in DMRG unlike the exponential growth in Wilson's standart renormalization group theory. Infinite system algorithm can be summarized in the following steps;

1. Having left and right blocks, form the left and right enlarged blocks. Note that left and right blocks are single sites at the very beginning of the algorithm.

2. Form the superblock Hamiltonian which is composed of right and left enlarged blocks.

3. Find the ground state eigenvector of the superblock Hamiltonian using a sparse matrix diagonalization routine. The corresponding eigenvalue found here gives the total energy of the system.

4. Using Eq.(3.8), form the reduced density matrices of the left and right halves of the system from the eigenvector found in the previous step.

5. Find the eigenvalues and eigenvectors of the reduced density matrices with a dense matrix diagonalization routine and form the truncation operators O_L and O_R from the highest weighted M eigenvectors of the density matrices as given in Eq.(3.13).

6. Using O_L and O_R, transform the left and right enlarged blocks and save the transformed blocks as new left and right blocks.

7. Using new left and right blocks, start from step 1 until the desired system size is reached.

The most difficult and time consuming part of the algorithm is the diagonalization of the superblock Hamiltonian to find its ground state. Thus it very important to make use of the symmetries of the system. For example total spin along z direction in an antiferromagnetic Heisenberg spin model commutes with the Hamiltonian so that Hamiltonian can be written in block diagonal form as we mentioned before. Thus it is easier to find the ground state of this section in the block diagonal form of the superblock. Similarly, commutation of total number operator with total Hamiltonian in Bose Hubbard model can be exploited in the diagonalization. For the diagonalization, one must use sparse matrix diagonalization routines such as Lanczos or Jacobi algorithms[50].

3.3.2 Finite System Algorithm

Finite system algorithm is used to find the ground state properties of finite systems up to extreme accuracy. The procedure of the infinite system algorithm is efficient for the search of properties in the thermodynamic limit. On the other hand, one may be interested in some finite system where infinite system algorithm gives relatively poor results. The difference between the two algorithms is in the formation of environment and system blocks. In the finite system algorithm one uses infinite system algorithm until the desired system length is obtained. This part of the finite system algorithm is called warm up. In this process blocks are saved as matrices in every iteration of warm up. If the length of the system is

L, we than have information of B_1^L,B_2^L,...,$B_{L/2}^L$ and B_1^R,B_2^R,...,$B_{L/2}^R$ at the end of warm up. After this point, the size of the superblock is kept fixed in further iterations so that system block size is increased whereas environment block size is decreased. For example, the next superblock diagonalization after warp up is of the form $B_{L/2}^L \otimes s \otimes s \otimes B_{L/2-2}^R$, where s represents the operators of single sites in between the blocks as before. The increase of the system size and the decrease of the environment size is done until the system size reaches $L-3$. That is, superblocks in the successive steps are

$$B_{L/2}^L \otimes s \otimes s \otimes B_{L/2-2}^R$$

$$B_{L/2+1}^L \otimes s \otimes s \otimes B_{L/2-3}^R$$

$$B_{L/2+2}^L \otimes s \otimes s \otimes B_{L/2-4}^R$$

$$\vdots$$

$$B_{L-3}^L \otimes s \otimes s \otimes B_1^R.$$

The system is swept to the right until the right block reduces to a single site. At each step the information for the right block is read from the disk which was saved in the warm up and new blocks for the left half are saved to the disk. For example, $B_{L/2+3}$ is obtained from the previous iteration by the truncation $O^\dagger[B_{L/2+2}^L \otimes s]O$ where O is the truncation operator obtained from the reduced density matrix of the left block as given in Eq.(3.13). Note that this density matrix is obtained from the diagonalization of the super block $B_{L/2+2}^L \otimes s \otimes s \otimes B_{L/2-4}^R$. When right block is a single site, the roles of left and right blocks are exchanged and same procedure is applied until left block becomes a single site. And finally, the roles of blocks are switched back again and left block is increased whereas right block is reduced until the symmetric configuration $B_{L/2-1}^L \otimes s \otimes s \otimes B_{L/2-1}^R$ is obtained. This whole operation,

. going right until the right end

. turning back and going left until the left end

. turning back and going right until the symmetric configuration $B_{L/2-1}^L \otimes s \otimes s \otimes B_{L/2-1}^R$

is called a complete sweep. After each sweep, accuracy increases and generally two or three sweeps are enough for the convergence.

3.4 Applications

3.4.1 Heisenberg Model

Heisenberg Spin model has been the first application of density matrix renormalization group theory because of its well established literature[51]. White applied DMRG to spin-1/2 and spin-1 model to illustrate the power of the method he developed[40].

The Hamiltonian for a one dimensional spin chain with nearest neighbor interactions is given by,

$$H = -J \sum_i \vec{S}_i \cdot \vec{S}_{i+1} = -J \sum_i S_i^x S_{i+1}^x + S_i^y S_{i+1}^y + S_i^z S_{i+1}^z \tag{3.15}$$

where i is the site index, $J < 0$ for the antiferromagnetic model and $J > 0$ for the ferromagnetic model. The spin operators satisfy the usual commutation relations,

$$[S^x, S^y] = iS^z$$

$\hbar$ is taken to be unity and x,y and z can be permuted in cyclic order. Commutator of the total Hamiltonian with S^z at a random site can be calculated as

$$\begin{aligned} [H, S_k^z] &= \sum_i [S_i^x S_{i+1}^x, S_k^z] + [S_i^y S_{i+1}^y, S_k^z] \\ &= -iS_{k+1}^x S_k^y - iS_{k-1}^x S_k^y + iS_k^x S_{k+1}^y + iS_k^x S_{k-1}^y. \end{aligned} \tag{3.16}$$

Summing this commutator over all k values gives zero which implies the conservation of the total angular momentum along z direction. That is, for $S_T^z = \sum_i S_i^z$,

$$[H, S_T^z] = 0.$$

In a similar fashion, it can be shown that $[H, \vec{S}^2] = 0$. These are the symmetries of the Hamiltonian which are extremely important in the implementation of DMRG.

Note that the second symmetry is very difficult to use in DMRG[44] but we will show the use of conservation of S_T^z in the following discussion.

Using the transformation $S^{\pm} = S^x \pm iS^y$ and taking $J = -1$ for simplicity, the Hamiltonian is written as

$$H = \sum_i \frac{1}{2}\left(S_i^+ S_{i+1}^- + S_i^- S_{i+1}^+\right) + S_i^z S_{i+1}^z. \tag{3.17}$$

3.4.1.1 Spin-1/2 System

For spin-1/2 system, the operators in above Hamiltonian are given by (for $\hbar = 1$),

$$S^+ = \begin{pmatrix} 0 & 1 \\ 0 & 0 \end{pmatrix} \quad S^- = \begin{pmatrix} 0 & 0 \\ 1 & 0 \end{pmatrix} \quad S^z = \frac{1}{2}\begin{pmatrix} 1 & 0 \\ 0 & -1 \end{pmatrix}.$$

Analytical solution of this system is available[52] as well as numerical solution via the Quantum Monte Carlo methods which makes it a strong benchmark for the implementation of any numerical method. In the following, we are going to show the first iteration of the infinite system algorithm as in the reference [53] but we will give results of each step as it appears on a computer (instead of analytical results of Malvezzi) for a demonstration.

At the beginning left and right blocks are single sites. Thus we define the Hamiltonian of the blocks as

$$H_L = H_R = \begin{pmatrix} 0 & 0 \\ 0 & 0 \end{pmatrix} \tag{3.18}$$

and other operators of the blocks are same as single site operators so that $S_L^+ = S_R^+ = S^+$ and $S_L^z = S_R^z = S^z$. One can obtain S^- operator for a block by taking the Hermitian conjugate of S^-, thus it is unnecessary to save them separately. Apart from the operators included in the interaction term, we need to keep matrices that give the total angular momentum (along z direction) of the blocks, separately. They are equal to S^z at the beginning so we save them as $S_L^T = S_R^T = S^z$. We can now start to follow the DMRG algorithm:

1. *Obtaining the left and right enlarged blocks*:

$$H_L^e = H_L \otimes I + S_L^+ \otimes S^- + S_L^- \otimes S^+ + S_L^z \otimes S^z$$

$$H_R^e = I \otimes H_R + S^+ \otimes S_R^- + S^- \otimes S_R^+ + S^z \otimes S_L^z$$

Other operators of the enlarged blocks are constructed as $(S_L^T)^e = S_L^T \otimes I + I_L \otimes S^z$, $(S_L^+)^e = I_L \otimes S^+$ and $(S_L^z)^e = I_L \otimes S^z$ where I stands for identity. Right block operators can be constructed similarly. To show the results of these operations, matrix representation of them are given as

$$H_L^e = \frac{1}{4}\begin{pmatrix} 1 & 0 & 0 & 0 \\ 0 & -1 & 2 & 0 \\ 0 & 2 & -1 & 0 \\ 0 & 0 & 0 & 1 \end{pmatrix}, \quad (S_L^T)^e = \begin{pmatrix} -1 & 0 & 0 & 0 \\ 0 & 0 & 0 & 0 \\ 0 & 0 & 0 & 0 \\ 0 & 0 & 0 & 1 \end{pmatrix}, \tag{3.19}$$

$$(S_L^z)^e = \frac{1}{2}\begin{pmatrix} 1 & 0 & 0 & 0 \\ 0 & 1 & 0 & 0 \\ 0 & 0 & -1 & 0 \\ 0 & 0 & 0 & -1 \end{pmatrix}, \quad (S_L^+)^e = \begin{pmatrix} 0 & 0 & 1 & 0 \\ 0 & 0 & 0 & 1 \\ 0 & 0 & 0 & 0 \\ 0 & 0 & 0 & 0 \end{pmatrix}.$$

Similar operators can be written for the right block. Note that Hamiltonian commutes with the total angular momentum matrix along the z direction which is seen from the block diagonal structure of the Hamiltonian. Keeping the states in accordance with the S_T^z provides this block structure in the further iterations as well.

2. *Construction of the superblock Hamiltonian*:

$$H_{sb} = H_L^e \otimes I_R^e + I_L^e \otimes H_R^e + (S_L^+)^e \otimes (S_R^-)^e + (S_L^-)^e \otimes (S_R^+)^e + (S_L^z)^e \otimes (S_R^z)^e$$

The dimension of the superblock is $dim(H_{sb}) = dim(H_L^e) \times dim(H_R^e) = 16$ which is the largest matrix throughout the iteration. Also, it is the matrix of which we need to find the ground state eigenvalue and eigenvector. Thus, it is necessary to employ symmetries here. It is known that ground state of Heisenberg spin system without magnetic field is in total spin-z zero symmetry sector of the Hamiltonian.

The dimension of this sector is 6, much less than the total dimension of the superblock 16. The superblock is found as (see [53] for details),

$$H_{sb} = \frac{1}{4}\begin{pmatrix} 1 & 0 & 0 & 0 & 2 & 0 \\ 0 & -3 & 2 & 2 & 0 & 2 \\ 0 & 2 & -1 & 2 & 0 & 0 \\ 0 & 2 & 0 & -1 & 2 & 0 \\ 2 & 0 & 2 & 2 & -3 & 0 \\ 0 & 2 & 0 & 0 & 0 & 1 \end{pmatrix}. \tag{3.20}$$

3. *Finding the ground state of the superblock*: The lowest eigenvalue of this matrix, found by a sparse matrix diagonalization routine is $E = -1.6160$ and corresponding eigenvector is

$$|\Psi\rangle = \begin{pmatrix} 0.1494 \\ -0.5577 \\ 0.4082 \\ 0.4082 \\ -0.5577 \\ 0.1494 \end{pmatrix}. \tag{3.21}$$

The state found above is called target state. Additional target states can be obtained here if necessary. For example exited states of the system here can be found by construction superblock in other nonzero spin-z sections which will be used later to show the energy gaps in the system.

4. *Formation of the reduced density matrices*: At this step the coefficients Ψ_{ij} in Eq.(3.9) can be written as $N_A \times N_B$ matrix. Thus density matrices of the left and right blocks can be written as $\rho^L = \Psi\Psi^\dagger$ and $\rho^R = (\Psi^\dagger\Psi)^T$, respectively.

Using the state given above, left block density matrix becomes

$$\rho^L = \begin{pmatrix} 0.0223 & 0 & 0 & 0 \\ 0 & 0.4777 & -0.4553 & 0 \\ 0 & -0.4553 & 0.4777 & 0 \\ 0 & 0 & 0 & 0.0223 \end{pmatrix}. \tag{3.22}$$

5. *Finding the eigenvalues and eigenvectors of the density matrix*: They are

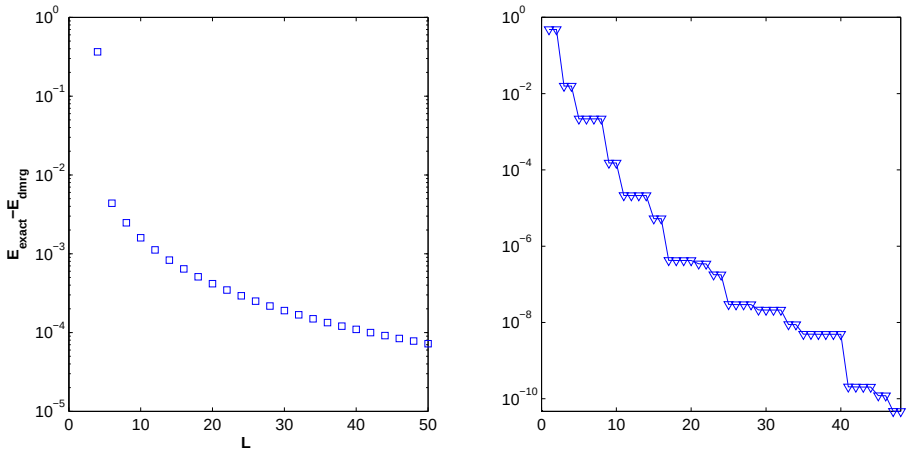

Figure 3.3: Convergence of the energy to the exact value is shown in the left pane and the decay of eigenvalues of the density matrix is in the right panel for M=24 states kept.

found to be 0.9330, 0.0223, 0.0223, 0.0223, respectively. The exponential decay of the eigenvalues can be seen here. Lets say we want to reduce the dimesion of the enlarged blocks to 2, then the transformation matrix is constructed from the highest two eigenvectors of the density matrix as

$$O^L = \begin{pmatrix} 0 & 0 \\ -0.7071 & -0.7071 \\ 0.7071 & -0.7071 \\ 0 & 0 \end{pmatrix} \tag{3.23}$$

where columns are the eigenvectors of ρ^L.

6. *Reduction of the enlarged block size to the beginning*:

$$H_L = O_L^\dagger H_L^e O_L = \begin{pmatrix} 0.2500 & 0 \\ 0 & -0.7500 \end{pmatrix}. \tag{3.24}$$

Other operators for the new blocks can be obtained similarly. After this step a new block composed of two sites is obtained and the procedure is repeated until the convergence is reached. Note that energy per site is calculated as one half of the difference in the eigenvalue of the superblock from one iteration to the next. The crucial part here is the projection of the superblock Hamiltonian to the desired total spin sector and formation of the density matrix from the ground state wave function. The reader can find a clear explanation at the reference [53] for both the construction of the superblock Hamiltonian and the use of its ground state ket to form the density matrices.

In Fig.3.3 we show the convergence of the energy for $M = 24$ states kept. It shows the strength of the method up to 10^{-4} precision for such a relatively small number of states. It is also seen that eigenvalues of the density matrix decays exponentially which is the reason of the good convergence. The degeneracies are seen as horizontally aligned markers which must be considered carefully while choosing the truncation parameter. For illustration purposes we have shown the

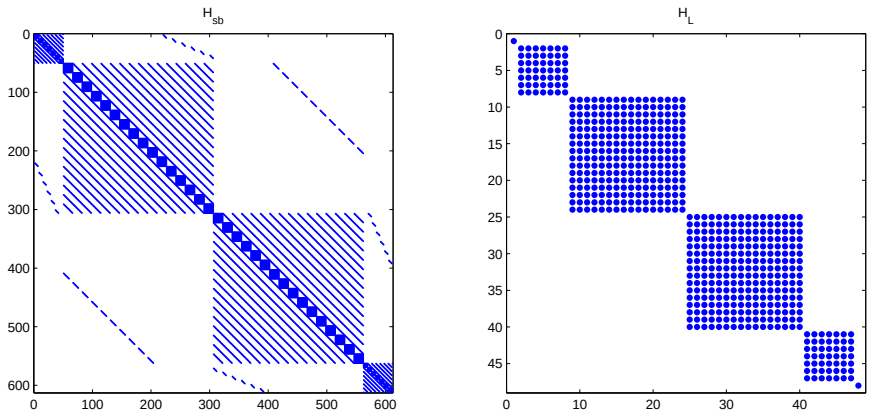

Figure 3.4: Sparseness of the superblock and the left enlarged block respectively.

block diagonal structure of the two matrices at the final iteration; superblock and

the left enlarged block. Superblock is the one corresponding to $S^z_T = 0$ symmetry section and the off-block diagonal terms come from the interaction between the left and right blocks. The block diagonal structure of the left enlarged block is seen in the right panel; each block inside the matrix corresponds to a different total spin.

3.4.1.2 Spin-1 System

Spin 1 system is modelled with the same Hamiltonian as in Eq.(3.17) where the relevant operators have the following matrix representations

$$S^+ = \begin{pmatrix} 0 & \sqrt{2} & 0 \\ 0 & 0 & \sqrt{2} \\ 0 & 0 & 0 \end{pmatrix} \quad S^- = \begin{pmatrix} 0 & 0 & 0 \\ \sqrt{2} & 0 & 0 \\ 0 & \sqrt{2} & 0 \end{pmatrix} \quad S^z = \begin{pmatrix} 1 & 0 & 0 \\ 0 & 0 & 0 \\ 0 & 0 & -1 \end{pmatrix}.$$

Haldane predicted that there must be a gap in the Heisenberg spin systems with interger spin whereas no gap exists in the half interger systems[54]. There is no analytical approach for the proof of this phenomenon and it was only shown by other numerical methods such as quantum Monte Carlo method by the time White developed the density matrix renormalization theory. He obtained the energy gap for spin-1 system better than any other numerical method in his work demonstrating the density matrix algorithm[40]. The algorithm for spin-1 system is a carbon copy of the procedure we demonstrated for spin-1/2 except the definition of the local site operators. To check the reliability of our DMRG code, we employed an exact diagonalization for some finite lattice, $L = 8$, and calculated a few lowest lying states, as White did in his presentation of first DMRG work[40]. Results of this comparison are given in Table 3.1. In Fig.3.5, we have shown the convergence of the energy calculated from our code and the eigenvalue spectrum of the density matrix. We have obtained ground state energy per site as $E/L = -1.40148$ by taking $M = 48$ states and $L = 100$ sites in the algorithm consistent with [42] up to 5 figures. Calculation of this energy took about two minutes on a moderate PC. For comparison, we show the gap in spin-1 and spin-1/2 systems in Fig.3.5. Note that the gap is defined to be the energy difference between the ground and first excited states for the spin-1/2 half system

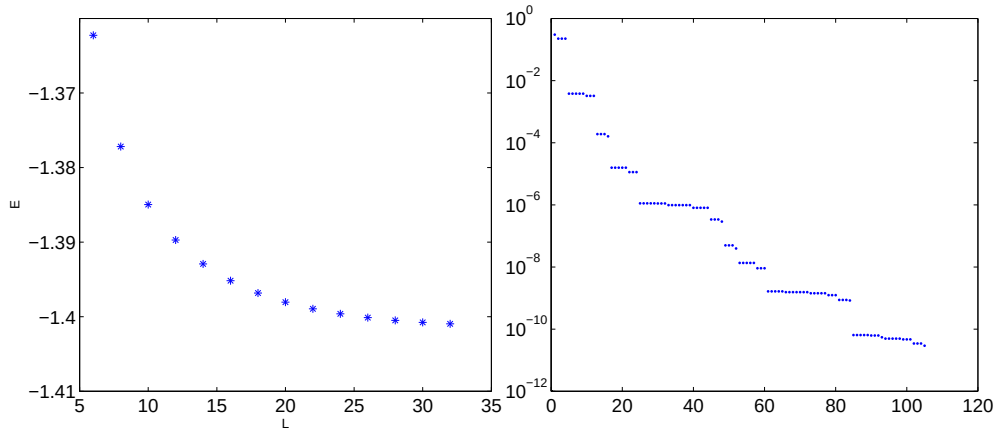

Figure 3.5: Energy per site as a function of system size is on the left for spin-1 system with open boundary conditions. On the right decay of density matrix eigenvalues are shown

Table 3.1: Difference between energy calculated from exact diagonalization and the energy of DMRG calculation for a finite size, L=8 site system.

M	$S_T = 0$	$S_T = 1$	$S_T = 2$
12	2.77×10^{-4}	1.42×10^{-3}	3.59×10^{-2}
24	2.59×10^{-6}	2.01×10^{-5}	9.15×10^{-4}
48	2.66×10^{-14}	1.24×10^{-14}	1.77×10^{-14}

whereas it is the difference between $S^z_T = 1$ and $S^z_T = 2$ symmetry sectors which correspond to the lowest two excited states for spin-1 system[51].

3.4.2 Bose-Hubbard Model

Bose Hubbard Hamiltonian is another model to which DMRG is applied. Although the initial applications were done for the fermionic Hubbard model[55],

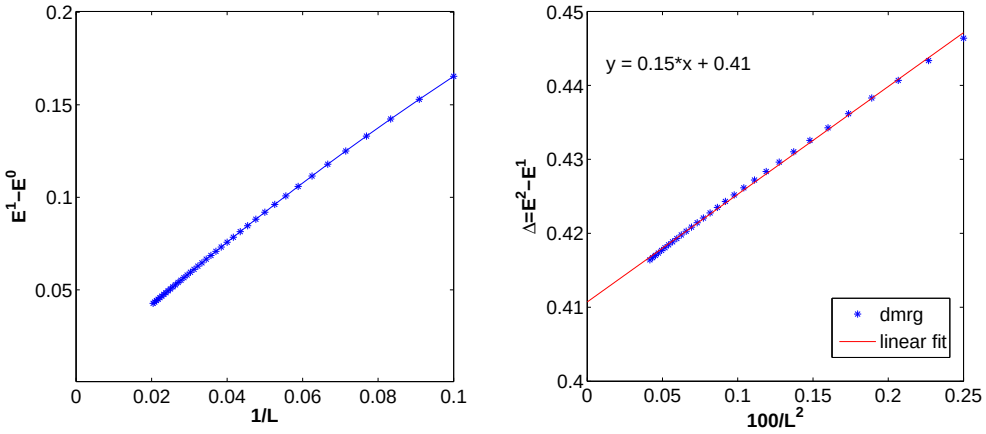

Figure 3.6: Haldane gap for spin-1/2 system as a function of inverse system size on the left and the one for spin-1 system as a function of inverse system size squared on the right. Gap is defined as the difference between ground state and the first excited state $\Delta_{1/2} = E^1 - E^0$ for spin-1/2 and difference between first and second excited states $\Delta_1 = E^2 - E^1$ for spin-1.

we are going to present the results for the bosonic case. Bose Hubbard Hamiltonian with nearest neighbor hopping, in one dimension is given by,

$$H = -J \sum_i a_i^\dagger a_{i+1} + a_{i+1}^\dagger a_i + \frac{U}{2} \sum_i n_i(n_i - 1) - \mu \sum_i n_i \tag{3.25}$$

where a_i and $a_i^\dagger$ are bosonic creation and annihilation operators defined on the local sites which satisfy the commutation relation $[a_i, a_j^\dagger] = \delta_{ij}$ and $n_i = a_i^\dagger a_i$ is the number operator, J is the hopping strength, U is the onsite interaction strength and μ is the chemical potential that controls the particle number fluctuation in the grand canonical ensemble.

This model has been studied by density matrix renormalization extensively and various properties has been explored. Mott-Superfluid-Bose glass phase diagram of this model is obtained with and without additional nearest neighbor hopping term by using both infinite and finite system algorithms[56, 57]. The model with and without disorder has been explored by a different group via DMRG[58] and phase diagrams are obtained for both extended Bose hubbard model[59] and under harmonic confinement[60]. In the following, we give summary and details,

when necessary, of some of these results and try to mention the basic methods and approaches.

3.4.2.1 Ground State

Action of creation, annihilation and number operators on a state ket $|n\rangle$ can be written as

$$\begin{aligned} a|n\rangle &= \sqrt{n}|n-1\rangle, \\ a^\dagger|n\rangle &= \sqrt{n+1}|n+1\rangle, \\ n|n\rangle &= n|n\rangle. \end{aligned} \tag{3.26}$$

Thus, one can write the infinite dimensional matrix representations of these operators. In DMRG implementation, however, it is required to cut these infinite dimensional operators at some point, say n_{max}, to use them in the algorithm. For $n_{max} = 4$, they take the form

$$a = \begin{pmatrix} 0 & 1 & 0 & 0 & 0 \\ 0 & 0 & \sqrt{2} & 0 & 0 \\ 0 & 0 & 0 & \sqrt{3} & 0 \\ 0 & 0 & 0 & 0 & 2 \\ 0 & 0 & 0 & 0 & 0 \end{pmatrix}, \quad n = \begin{pmatrix} 0 & 0 & 0 & 0 & 0 \\ 0 & 1 & 0 & 0 & 0 \\ 0 & 0 & 2 & 0 & 0 \\ 0 & 0 & 0 & 3 & 0 \\ 0 & 0 & 0 & 0 & 4 \end{pmatrix}. \tag{3.27}$$

Having these finite matrices, its a straightforward application to implement usual DMRG algorithm. To use the conservation of total number of particles, its possible to drop the term with chemical potential and work in canonical ensemble. Hamiltonian for a single site will be $h_{site} = n(n-I)/2$ where I is identity matrix and U is taken to be unity. Thus, it will be similar to the scheme presented before, except single site Hamiltonians are no longer zero. We follow the standart recipe: enlargement of the blocks beginning from a single site, construction of the superblock and finding the ground state to form the density matrices and finally making truncations when necessary.

For the use of symmetries, it can be shown that $[H, N] = 0$ where N is the

total number operator given as

$$N = \sum_i n_i \tag{3.28}$$

Thus its the number operator that will be the basis for the construction of blocks and enlarged blocks. To find the ground state of a system with known length, it is necessary to set total number of particles. For example, to find ground state in a Mott region, where there is one particle per site, we need to make projections in the formation of superblock accordingly. For example, in the first iteration projection will be made onto $N = 4$ sector where the superblock is composed of 4 sites . In the next iteration, where superblock this time has six sites, projection will be made onto $N = 6$ sector, and so on. Energies of the defect states can be found similarly. For instance, to find energy with one hole (particle), superblocks will be projected onto $L - 1$ $(L + 1)$ particles sector, where L is the number of sites in the superblock. It is important to note that, accuracy of the results might be poor for large differences between the length of the system (total number of sites) and total number of particles. For the solution of one particle-hole defect states, infinite system algorithm gives pretty good results, however it is necessary to use the finite system algorithm for many particle-hole states.

In Fig.3.7, we have shown output of our DMRG code. Ground state energies per particle have been plotted against the system size for Mott State, when there is one particle per site, together with the additional one hole and one particle states. The figure is plotted for two different values of the hopping strength. For the small values of hopping strength, system is expected to be in Mott insulator state that has a finite gap with particle hole excitations. As the hopping strength increased, system undergoes a phase transition to the superfluid phase characterized by gapless particle hole excitation. This transition is seen in Fig.3.7 so that, the finite gap appearing for small J (left panel), disappears for a large J (right panel).

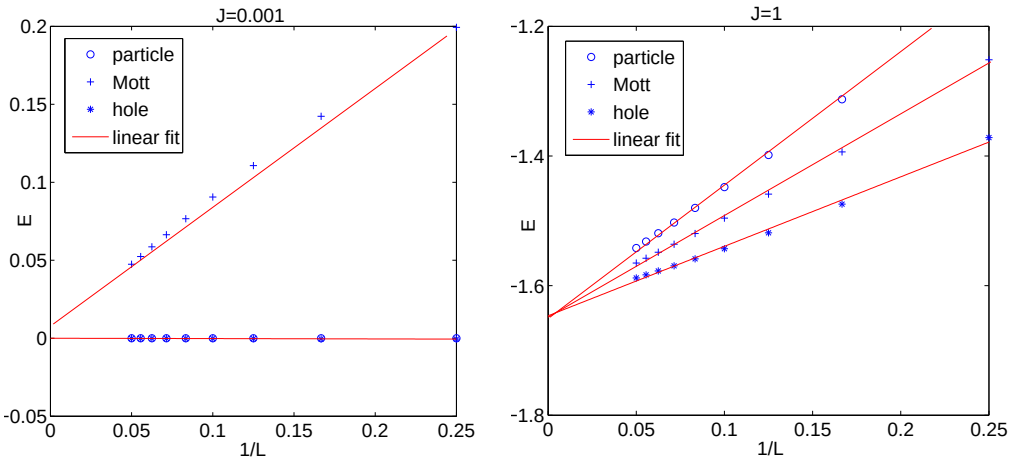

Figure 3.7: Ground state energies versus inverse system size of Bose Hubbard model for Mott state and particle-hole defect states for two different values of hopping parameter,$J = 0.001$ (on left) and $J = 1$ (on right). Red straight lines are linear fits to DMRG points.

3.4.2.2 Superfluid-Mott Insulator Transition

The precision of the calculated energies with DMRG strongly depends on the decay of density matrix eigenvalues. Carefull attention must be paid on the determination of truncation parameter so that weighted majority of eigenvalues of density matrix must be in the range of states that are kept at each iteration. For the Bose Hubbard model treated here, correlations in the Mott insulator region are small and the particles are well localized in sites if hopping strength is weak. As the strength of hopping is increased, particles will loose their localization and start to hop around. In this regime, the correlations are no more weak and the number of states that are effective in the system increases. This can be seen in Fig.3.8, where eigenvalue spectrum of the density matrix is shown for two different hopping strengths. Thus the accuracy of the results decreases with the same number of states kept while the hopping strength increases. One needs to increase the number of states to obtain the same accuracy. In our calculations, we calculated the error, $\epsilon_M = 1 - \sum_{\alpha=1}^{M} \lambda_\alpha$, to be order of 10^{-5} for $J = 1$ and 10^{-10} for $J = 0.001$ with $M = 30$ states kept.

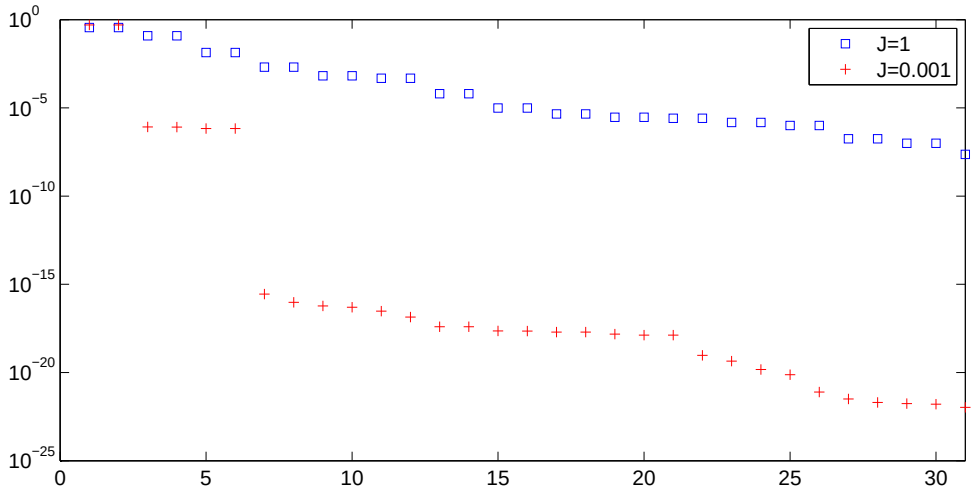

Figure 3.8: Eigenvalue spectrum of the density matrices in Bose Hubbar model DMRG for two different values of hopping strength.

Superfluid to Mott insulator transition is characterized by the existence of a finite gap in the Mott region. The gap for a finite system of length L is defined as,

$$G_L = E_L(N+1) + E_L(N-1) - 2E_L(N) \tag{3.29}$$

where $N = L$ for $\rho = 1$ corresponding to one particle per site. In the thermodynamic limit, this gap is expected to be nonzero for a Mott insulator and zero for a superfluid. On the other hand, it is not possible to work on infinite systems that will mimic out the properties in the thermodynamic limit, by using density matrix renormalization group theory. One way to tackle this problem is looking at the values of LG_L instead of G_L[58, 61]. Since gap is approaching zero while system size goes to infinity, their product LG_L is expected to go to a constant in thermodynamic limit. Thus if we plot LG_L versus J, the hopping strength, for different system sizes, curves of different sized systems are expected to coalesce at the point where phase transition occurs. This is shown in Fig.3.9 where curves overlap above a critical value J_c. From the figure, we can say that the tip is at about 0.28, which is very close to calculated J_c with other approaches[56, 57].

The transition found above is Kosterlitz-Thouless type which comes from the quantum phase fluctuations in the system while the particle density is kept

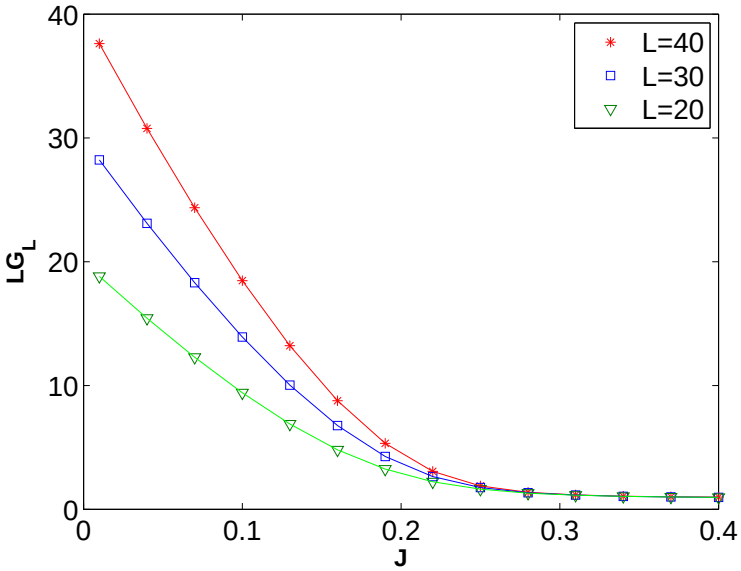

Figure 3.9: Gap multiplied by size vs hopping strength for different system sizes with $M = 30$ states kept. Coalescence of curves for different lengths shows the transition to superfluid. Transition is Kosterlitz-Thouless type.

constant. It is possible to obtain phase boundaries of Mott insulator region coming from the density or number fluctuations in the system[56, 57]. Location of this generic transition can be found by looking at the necessary energies to add or subtract a particle from the system in Mott insulator, i.e

$$\begin{aligned} \mu_c^p &= E_p - E_m \\ \mu_c^h &= -E_h + E_m \end{aligned} \tag{3.30}$$

where μ is the chemical potential and E_p, E_h are the energies with one additional particle, hole respectively and E_m is the Mott insulator ground state energy. By calculating these three energies the full phase boundary of the Mott Insulator region can be obtained which is shown in Fig.10. It can be seen from the figure that the tip of the insulator region do not close as J is increased, because the transition is different at this point. They are expected to overlap in the thermodynamic limit. This can be seen by running the same code for a larger system size so that, the lines above and below will be closer to each other for larger L. Combining the previous method shown in Fig.3.9, we can say that boundary at

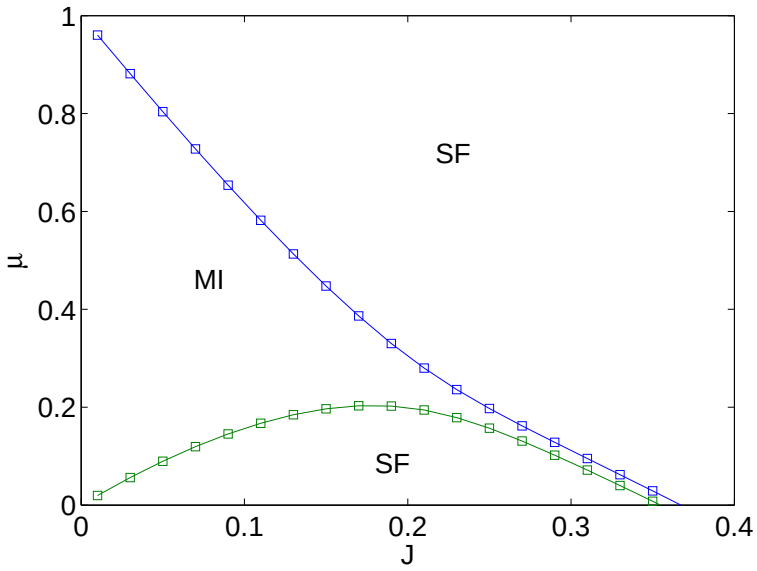

Figure 3.10: Phase diagram of one dimensional Bose hubbard model with onsite interaction. $M = 30$ states are kept in the dmrg iteration for a system of size $L = 50$. The BKT phase transition is not seen because of the method used which is mentioned in the text.

this point is expected to be $J_c = 0.28$.

3.5 Conclusion

In this chapter, we summarize the steps of density matrix renormalization group theory from the beginning. Very basic points of DMRG and details that were difficult for us to understand are explained as we worked through the implementation of the algorithm. It is hoped that either the explanations given in the text or the references given there will be helpful for a beginner. We tried to include all the references that are used so that the reader can see them whenever necessary.

The basic theory of the DMRG, built on the density matrix formalism, is presented and all steps required to write a program are given. To show the mechanism and also the strength of the method, two different applications are given; Heisenberg spin model and Bose Hubbard model. We skipped two very

important parts: the observable expectations and the boundary conditions. The method we have given is the so called open boundary consitions. Other boundary conditions like periodic, soft or twisted is not mentioned. Reader might need to see refences to work on these and a lot more topics that we did not mention here.

The most important problem of DMRG is that it can only be used for one dimensional systems. If someone is working in one dimension or quasi-one dimension, DMRG is the most reliable method that can be used. It does not require any information about the previous renormalization theories which makes it quite accessible.

Chapter 4

Two Leg Bose Hubbard Model

In this chapter, two leg Bose Hubbard ladder under a uniform magnetic field is studied. The model is introduced within the formalism of Bose Hubbard Hamiltonian and system parameters are defined below. Then different analytical and numerical approaches are performed to study the model. In Section 4.1 noninteracting particles on two legged ladder are studied and single particle spectrum of the model is obtained. A critical magnetic field is found such that system displays different properties above and below this critical value of the field. In Section 4.2, interacting many particles on the two leg ladder are analyzed by use of Gross Pitevskii approximation. An order parameter is defined and the resulting equation of motion is solved analytically to obtain the dispersion relation of interacting many particles. In Section 4.3 superfluid to Mott insulator transition is studied and Mott insulator phase boundary is obtained by using a variational meanfield theory. In Section 4.4, the same phase diagram is obtained by strong coupling perturbation and the results of the two different methods are compared. In the last part, Section 4.5 and 4.6 exact behavior of the system is studied using density matrix renormalization group (DMRG) theory .

System Hamiltonian is given by

$$\begin{aligned} H = & - t\sum_i e^{-i\alpha}a_i^\dagger a_{i+1} + e^{i\alpha}b_i^\dagger b_{i+1} + a_i^\dagger b_i + H.C. \\ & + \frac{U}{2}\sum_i n_i^a(n_i^a-1) + n_i^b(n_i^b-1) - \mu\sum_i n_i^a + n_i^b \end{aligned} \tag{4.1}$$

where a_i ($a_i^\dagger$) are bosonic annihilation (creation) operators for upper leg, b_i ($b_i^\dagger$) are bosonic annihilation (creation) operators for lower leg, $n_i^a = a_i^\dagger a_i$ and $n_i^b = b_i^\dagger b_i$ are number operators, t is the hopping strength, U is the onsite interaction strength and μ is the chemical potential. We are assuming a homogeneous system that has up-down symmetry for zero magnetic field, so t, U and μ are taken identical for each leg. The phase difference α gained by the hopping from position $\mathbf{r_i}$ to $\mathbf{r_j}$ is calculated from

$$\alpha = \int_{\mathbf{r_i}}^{\mathbf{r_j}} d\mathbf{r}\cdot\mathbf{A}(\mathbf{r}) \tag{4.2}$$

where and $\mathbf{A}$ is the vector potential satisfying $\nabla\times\mathbf{A} = \mathbf{B}$ and $\mathbf{B}$ is the magnetic field perpendicular to two leg plane. We use Landau gauge $\mathbf{A} = -By\hat{x}$ which satisfies $\mathbf{B} = B\hat{z}$. Note that this gauge does not brake the translational invariance along x-direction. Thus the exponent in Eq.(4.1) is calculated from Eq.(4.2) as $\alpha = \pi\phi/\phi_0$ where ϕ is the flux passing through each plaquette and $\phi_0 = hc/e$ is the flux quantum. For a two dimensional system, ϕ/ϕ_0 is taken to be a rational number p/q and the system is assumed to be q site periodic along y-direction which partially fixes the symmetry broken by the gauge. Our system does not require such a constraint so that α/π can be any real number between zero and one.

4.1 Single Particle Spectrum

We first study the solution for non-interacting particles, $U = 0$, to obtain the single particle spectrum. Single particle solution of the two dimensional Bose Hubbard model under magnetic field ends up with a difference equation, called Harper's equation, that gives a fractal energy spectrum known as Hofstadter butterfly. In the two leg ladder system, solution is much easier because of the

simpler symmetry of the system. Using the translational invariance along x-direction, Fourier components of the field operators are written as,

$$a_j = \frac{1}{\sqrt{L}} \sum_k a_k e^{ikja}, \quad b_j = \frac{1}{\sqrt{L}} \sum_k b_k e^{ikja} \tag{4.3}$$

where L is the length of the system and Fourier components satisfy the commutation $[a_k, a_{k'}^\dagger] = \delta_{kk'}$ and $[b_k, b_{k'}^\dagger] = \delta_{kk'}$, all other commutators being zero. Using these transformations in Eq.(4.1), the Hamiltonian is written in momentum space as,

$$H_{sp} = -t \sum_k A_k a_k^\dagger a_k + B_k b_k^\dagger b_k + a_k^\dagger b_k + b_k^\dagger a_k \tag{4.4}$$

where $A_k = 2\cos(ka - \pi\phi/\phi_0)$ and $B_k = 2\cos(ka + \pi\phi/\phi_0)$. One can define the following Bogoliubov transformation for the diagonalization of the Hamiltonian

$$\alpha_k = \cos\theta_k a_k + \sin\theta_k b_k, \quad \beta_k = -\sin\theta_k a_k + \cos\theta_k b_k. \tag{4.5}$$

It can be shown that this transformation is canonical and diagonalizes the Hamiltonian for $\theta = \frac{1}{2}\arctan(\frac{2}{A_k - B_k})$. Thus the energy eigenvalues of this Hamiltonian will have the form

$$\epsilon_{1,2} = -\frac{A_k + B_k}{2} \mp \frac{1}{2}\sqrt{(A_k - B_k)^2 + 4}. \tag{4.6}$$

In Fig.4.1, the dispersion relation in the first Brillouin zone is shown, for zero and non-zero magnetic fields. It is seen that, as the strength of the field increases, the energy band minimum in the dispersion shifts from $k = 0$ to two nonzero k values which are degenerate and symmetric around the origin. Thus upon increasing the magnetic field above a critical value, the system no longer bears stationary solutions, but has travelling waves to the left or right. The critical value of this magnetic field is found from the dispersion relation Eq.(4.6) by equating the second derivative to zero with respect to k around $k = 0$. The critical value of the field is $\alpha_{cr} = cos^{-1}[-\sqrt{17}/4 + 1/4]$ which is numerically equal to 0.2148 or 0.7852 (0.7852 comes from the mirror symmetry of the energy spectrum around $\alpha = 0.5$). Above 0.2148 and and below 0.7852, $k = 0$ state changes from being the energy minimum to a local energy maximum.

Another observation from the Fig.4.1 is that, for zero magnetic field, there is no gap between the valence and the conduction band. On the other hand,

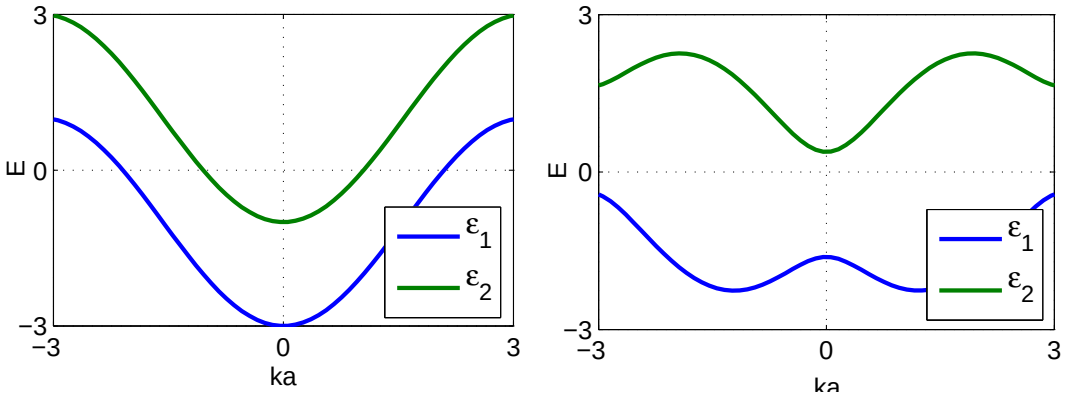

Figure 4.1: Single particle band diagram two leg ladder under magnetic field. Left pane is plotted for $\alpha = 0$ whereas right pane is for $\alpha = 0.4$. The band gap between the conduction and the valance bands is zero for the left which is nonzero for the right.

for $\alpha = 0.4$ there is a finite band gap between these two energy bands. Thus, introducing a magnetic field of a certain strength eventually gives rise to the appearance of a gap in the spectrum. In Fig.4.2, we have plotted minima and maxima of valence and conduction bands as a function of the magnetic field. This plot can be regarded as 'Hofstadter butterfly' of the two legged quasi-one dimensional system. From Fig.4.2 it is seen that the one and the largest gap area of the spectrum is squeezed between $\alpha = 1/3$ and $\alpha = 2/3$ among the full spectrum that is symmetric around $\alpha = 0.5$.

4.2 Gross-Pitaevskii Approximation

For small values of the onsite interaction strength, the system is essentially in the superfluid state, mostly governed by the hopping term in the Hamiltonian. This enables us to define an order parameter which is the expectation value of the field operator. Thus, assuming that the condensate is slowly varying over the

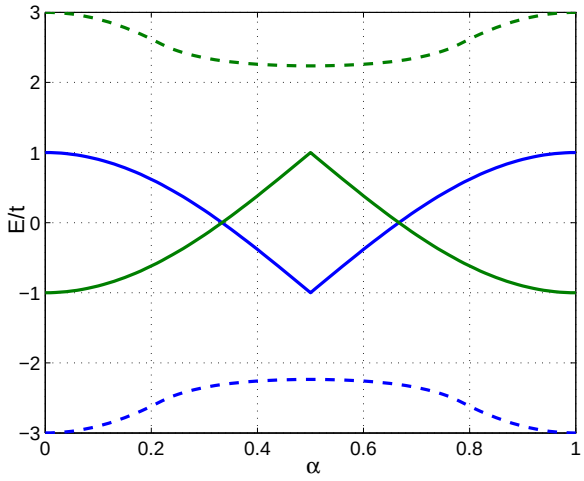

Figure 4.2: Band minimums (dashed blue for the conduction band and solid green for the valance band) and band maximums (solid blue for the conduction band and dashed green for the valance band) as a function of magneticfield. Analog of Hofstadter butterfly for two leg ladder. A finite gap between conduction and valance band appears at $\alpha = 1/3$

system, one can make the substitution

$$\begin{aligned} a_i &\rightarrow \langle a_i \rangle = \psi_i \\ b_i &\rightarrow \langle b_i \rangle = \phi_i \end{aligned} \tag{4.7}$$

where Hermitian conjugates of the field operators directly follow from this as $a_i^\dagger = \psi_i^*$ and $b_i^\dagger = \phi_i^*$. ψ_i's and ϕ_i's are classical macroscopic quantities which are to be chosen carefully. Condensation does not necessarily occur at $k = 0$ stationary state, following the discussion in the previous section. Thus both amplitude and the phase of these classical fields is time and position dependent[62]. As a result, behavior of the condensate order parameter is different below and above the critical magnetic field which requires one to define different order parameters for each region.

Making the substitution in Eq.(4.8) with the Hamiltonian in Eq.(4.1), the

following energy functional is obtained (take $t = 1$ for simplicity);

$$\begin{aligned} E[\{\psi_i\},\{\phi_i\}] = & - \sum_j e^{-i\alpha}\psi_j^*\psi_{j+1} + e^{i\alpha}\phi_j^*\phi_{j+1} + \psi_j^*\phi_j + c.c. \\ & + \frac{U}{2}\sum_j \psi_j^*\psi_j(\psi_j^*\psi_j - 1) + \phi_j^*\phi_j(\phi_j^*\phi_j - 1) - \mu\left(|\psi_i|^2 + |\phi_i|^2\right). \end{aligned} \tag{4.8}$$

Variations of the energy functional around the wavefunctions gives the dynamics of the system, i.e. $i\hbar\frac{\partial\psi_i}{\partial t} = \frac{\delta E}{\delta\psi_i{}^*}$ and $i\hbar\frac{\partial\phi_i}{\partial t} = \frac{\delta E}{\delta\phi_i^*}$. These expressions give two coupled equations,

$$\begin{aligned} i\hbar\frac{\partial\psi_j}{\partial t} &= -\left[e^{-i\alpha}\psi_{j+1} + \phi_j + e^{i\alpha}\psi_{j-1}\right] + U|\psi_j|^2\psi_j - \left(\frac{U}{2} + \mu\right)\psi_j \\ i\hbar\frac{\partial\phi_j}{\partial t} &= -\left[e^{i\alpha}\phi_{j+1} + \psi_j + e^{-i\alpha}\phi_{j-1}\right] + U|\phi_j|^2\phi_j - \left(\frac{U}{2} + \mu\right)\phi_j \end{aligned} \tag{4.9}$$

which are nonlinear difference equations. These equations are nonlinear Schödinger equations coupled to each other in discrete form, that is why we call this section Gross-Pitaevskii approximation. Zeroth order terms $\psi_j = \phi_j = \sqrt{n}$ will give the chemical potential as $\mu = -(2\cos\alpha + 1) + 0.5U(2n - 1)$ which satisfies the previously obtained dispersion relation in Eq.(4.6) for $U = 0$. For a higher order approximation, small oscillations around this equilibrium value are considered,

$$\begin{aligned} \psi_j &= \sqrt{n} + Ae^{i(\mathbf{k}.\mathbf{r_j} - wt)} + B^*e^{-i(\mathbf{k}.\mathbf{r_j} - wt)} \\ \phi_j &= \sqrt{n} + Ce^{i(\mathbf{k}.\mathbf{r_j} - wt)} + D^*e^{-i(\mathbf{k}.\mathbf{r_j} - wt)} \end{aligned} \tag{4.10}$$

where A, B, C, D are small complex parameters and $\mathbf{r_j}$ is a vector from the origin to a lattice point and k being the reciprocal lattice vector. Inserting these wavefunctions into Eq.(4.10) and equating the exponents, the following determinant is obtained for the existence of a nontrivial solution of the coefficients;

$$\begin{vmatrix} K + \hbar\omega & -Un & 1 & 0 \\ -Un & L - \hbar\omega & 0 & 1 \\ 1 & 0 & L + \hbar\omega & -Un \\ 0 & 1 & -Un & K - \hbar\omega \end{vmatrix} = 0$$

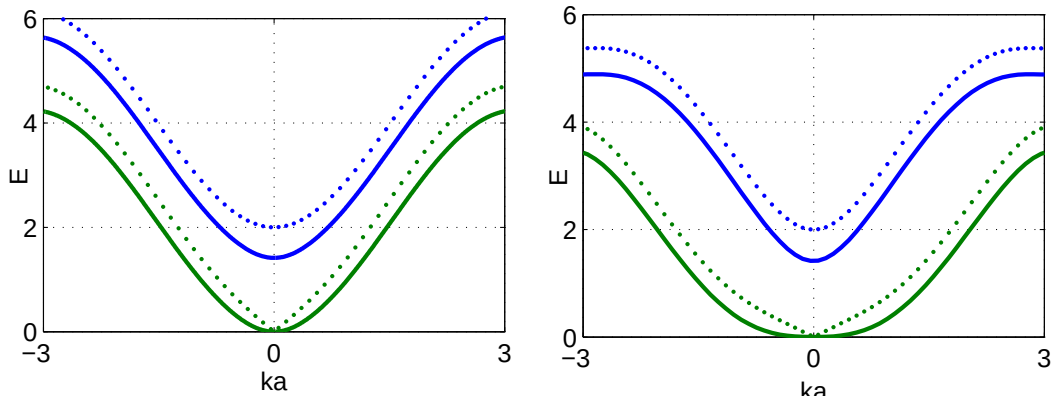

Figure 4.3: Band diagrams for two leg ladder with onsite interactions calculated from the Gross Pitaevskii approximation. Solid lines are for $U = 0$ and dotted lines are for $U = 0.5$. Left panel is for zero magnetic field and the right panel is for $\alpha = 0.2$

where $K = 2cos(ka - \alpha) - 2cos(\alpha) - Un - 1$ and $L = 2cos(ka + \alpha) - 2cos(\alpha) - Un - 1$. Equating the determinant to zero, dispersion relation is obtained from the solution of this matrix which is plotted in Fig.4.3.

In Fig.4.3, solid lines are for $U = 0$ and dotted lines are for $U = 0.5$. Non interacting case is in agreement with the band diagram in Fig.4.1 apart from an additive constant. The effect of interactions is to shift the band upward for nonzero k whereas the band minimum persists on $k = 0$. Around $k = 0$, interaction sharpens the band and provides a cusp like shape. On the other hand, increase of the magnetic field, on the right panel, causes a smoother band so that the linearity of the dispersion is lost. The expansion of the wave function in Eq.(4.10) fails above the critical magnetic field, giving imaginary frequencies which implies an unstable solution. We use this property to see the change of the critical field with the interaction strength. In Fig.4.4, the change of the critical magnetic field with the strength of the interaction is shown. It can be seen that, $U - \alpha_c$ relation is almost linear for small interaction strengths but it saturates for strong interactions. Note that results of the strong onsite interaction are not reliable because; firstly, the Gross Pitaevskii approximation is no more valid in this region, secondly, attained magnetic field requires a wave function different from the one in Eq.(4.10). Thus, we conclude that the critical magnetic

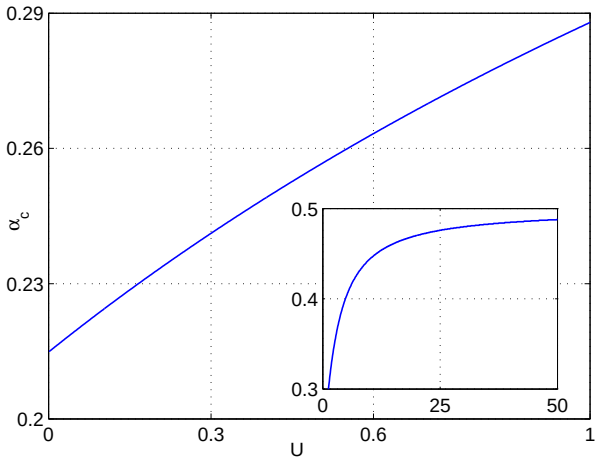

Figure 4.4: Change of critical magnetic field with the increase of interaction strength for low values of U, that is $Un/t < 1$. Plot is scaled with $t = 1$ and $n = 1$. In the limit $U \to 0$, α_c goes to the previously obtained value from the single particle solutions. Inset shows the behavior for large values of U, which is not reliable because of strong interactions.

field increases linearly for weak interactions, that is for $U < t/n$. Increase of interactions promotes solutions that are uniform through the lattice. That means, to minimize the interaction energy, it is better to distribute particles uniformly on the lattice. This makes wave functions proportional to $\sqrt{n}$ more stable which means that the onsite interaction increases the critical magnetic field strength.

4.3 Variational Mean Field Approach

In this section, we determine the Mott insulator phase boundary for different values of the parameters t, μ and α. It is convenient to scale the Hamiltonian in Eq.(4.1) with $U = 1$. In the perfect Mott insulator phase, each site has a localized wavefunction and system is decoupled so that there are precisely n_0 particles per site and the corresponding wavefunction is shown by $|n_0\rangle_i$ in the Fock basis. Allowing small variations around this equilibrium, the local wave functions take the form $\Delta_i|n_0 - 1\rangle_i + |n_0\rangle_i + \Delta_i'|n_0 + 1\rangle_i$ where Δ_i and Δ_i' are variational parameters to be determined. In general for a two dimensional Bose Hubbard

model, these parameters are assumed to be real since complex parameters are expected to increase the energy[38] but for the two leg Bose Hubbard ladder, real Δ assumption is found to give unbounded Mott insulator phase region. Thus, the wave function is generalized to include complex values and the following Gutzwiller ansatz is defined for local wave functions,

$$\begin{aligned} |G\rangle_a^k &= \Delta_a^k e^{i\theta_k}|n_0-1\rangle_a^k + |n_0\rangle_a^k + (\Delta_a^k)' e^{i\theta_k}|n_0+1\rangle_a^k \\ |G\rangle_b^k &= \Delta_b^k e^{i\theta_k}|n_0-1\rangle_b^k + |n_0\rangle_b^k + (\Delta_b^k)' e^{i\theta_k}|n_0+1\rangle_b^k \end{aligned} \tag{4.11}$$

where subscripts a and b stand for upper and lower legs respectively, superscripts are site indices and θ_k is the additional variational parameter to be determined. Having these local kets, the wave function for a rung becomes $|G_r\rangle^k = |G\rangle_a^k |G\rangle_b^k$ and the total wavefunction of the system can be written as $|\Psi\rangle = \prod_k^N |G\rangle_a^k |G\rangle_b^k$. This form of the wave function decouples the Hamiltonian in Eq.(4.1) and the total energy of the system can be written as $E = N\varepsilon$, where ε is the variational energy per a rung given by,

$$\varepsilon = \frac{\langle G_r|H|G_r\rangle}{\langle G_r|G_r\rangle}. \tag{4.12}$$

Keeping terms up to second order in Δ, the following expression is obtained for the energy per a rung

$$\begin{aligned} \varepsilon = &- 2t\cos(\alpha+\theta)\left[\Delta_a^2 n_0 + (\Delta_a')^2(n_0+1) + 2\sqrt{n_0(n_0+1)}\Delta_a\Delta_a'\right] \\ &- 2t\cos(\alpha-\theta)\left[\Delta_b^2 n_0 + (\Delta_b')^2(n_0+1) + 2\sqrt{n_0(n_0+1)}\Delta_b\Delta_b'\right] \\ &- 2t\left[\Delta_a\Delta_b n_0 + \Delta_a'\Delta_b'(n_0+1) + \sqrt{n_0(n_0+1)}(\Delta_a\Delta_b' + \Delta_a'\Delta_b)\right] \\ &+ \left[(1-n_0)(\Delta_a^2+\Delta_b^2) + n_0(n_0-1) + n_0((\Delta_a')^2 + (\Delta_b')^2)\right] \\ &+ \mu\left[(\Delta_a^2 - (\Delta_a')^2) + (\Delta_b^2 - (\Delta_b')^2) - 2n_0\right] \end{aligned} \tag{4.13}$$

where the site indices are not written for compactness. This energy is minimized with respect to five variational parameters; four of them coming from Δ's and one from the phase θ. The first minimization is done on Δ's. For the energy in Eq.(4.14) to be a minimum, the Jacobian matrix should be positive definite (all of the eigenvalues are positive). At the point where the determinant of the Jacobian matrix is zero, the energy in Eq.(4.14) is no more a minimum of energy which means that the system is not Mott insulator anymore. Jacobian matrix is

calculated as,

$$\begin{aligned}\mathbf{J} = \quad & -2t \quad \begin{pmatrix} n_0\mathbf{F} & \sqrt{n_0(n_0+1)}\mathbf{F} \\ \sqrt{n_0(n_0+1)}\mathbf{F} & (n_0+1)\mathbf{F} \end{pmatrix} \\ & +2 \quad \begin{pmatrix} (1-n+\mu)\mathbf{I} & 0 \\ 0 & (n-\mu)\mathbf{I} \end{pmatrix}\end{aligned} \tag{4.14}$$

where $\mathbf{I}$ is 2×2 identity matrix and $\mathbf{F}$ has the same structure with the single particle Hamiltonian in Eq.(4.4), which is

$$\mathbf{F} = \begin{pmatrix} 2\cos(\alpha+\theta) & 1 \\ 1 & 2\cos(\alpha-\theta) \end{pmatrix}. \tag{4.15}$$

Positive definiteness of a matrix requires all eigenvalues to be positive. Thus the minimum eigenvalue of the Jacobian matrix in Eq.(4.15) is found and equated to zero to find the phase boundary of Mott insulator region. To find the eigenvalues, we use the following[38]; let $\lambda_{\mathbf{F}}$ and $\vec{u}$ be eigenvalues and eigenvectors of $\mathbf{F}$ respectively, then one can apply an ansatz of the form

$$\vec{v} = \begin{pmatrix} a\vec{u} \\ b\vec{u} \end{pmatrix}$$

and solve the eigenvalue equation $\mathbf{J}\vec{v} = \lambda\vec{v}$. The eigenvalues of Jacobian matrix are found as

$$\begin{aligned}\lambda_{1,2} &= 1 - t\lambda_{\mathbf{F}}(2n_0+1) \\ &\pm \sqrt{(1-t\lambda_{\mathbf{F}}(2n_0+1))^2 + 4t\lambda_{\mathbf{F}}(\mu+1) - 4(n_0-\mu)(1-n_0+\mu)}.\end{aligned} \tag{4.16}$$

Setting the smaller eigenvalue to zero and solving the corresponding equation for t, the following relation is found for the boundary of Mott phase,

$$t_c = \frac{(n_0-\mu)(1-n_0+\mu)}{(\mu+1)\lambda_{\mathbf{F}}}. \tag{4.17}$$

Note that the eigenvalues $\lambda_{\mathbf{F}}$ in Eq.(4.17) are the same with energies in Eq.(4.6). To plot the Mott phase boundary, we minimize the lowest eigenvalue with respect to θ for each value of the magnetic field α.

In Fig.4.5, the result of the minimization is shown, which specifies a certain region for Mott insulator phase. The complex variable θ plugged in the ansatz

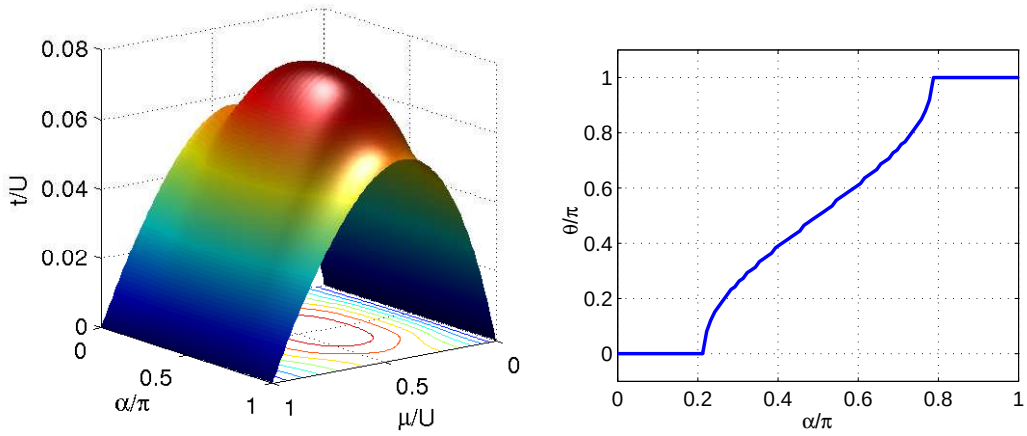

Figure 4.5: Mott phase boundary is shown on the left as a function of magnetic field strength and the chemical potential. Unlike two dimensional case, boundary is perfectly smooth. On the right, result of the minimization of the energy with respect to phase parameter θ in Eq.(4.12) is shown. It is seen that above the critical magnetic field, the minimum energy ansatz bears complex amplitudes as in the case of single particle solution.

Eq.(4.12) follows the similar structure with that of the single particle solution; above the critical magnetic field it takes nonzero values as shown on the right panel of Fig.4.5. Our results are exact within mean field theory. On the other hand, the meanfield theory applied to our system is not expected to give good results. This approach essentially decouples the hopping term in Eq.(4.1) and gives it a mean field behavior. This decoupling is bad for low dimensions, especially for one dimensional systems since correlations are more dominant in 1D relative to two and three dimensions. Thus, this calculation is not expected to give accurate results. The determination of the tip of the Mott lobe where BKT(Berezinskii, Kosterlitz, Thouless) transition takes place and the calculation of the shape of the Mott insulating region around this point is not reliable. On the other hand, a rough sketch of the topology of the Mott insulator region is obtained within this method. Additionally, for small values of the hopping strength, where the correlations are diminished, the results are expected to be reliable.

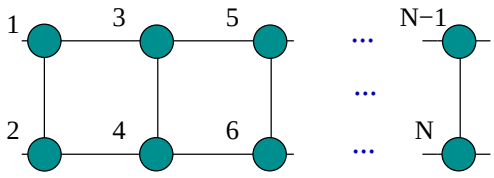

Figure 4.6: Labelling of sites in two leg ladder for the calculation of strong coupling expansion

4.4 Strong Coupling Expansion

In the strong coupling perturbative expansion, the hopping term is taken to be weak and considered as a perturbation. The Mott insulator state is characterized by a finite gap for particle-hole excitations whereas this gap vanishes for the superfluid phase[18]. Thus if the energies of a system with n_0 particles per site (called Mott state) and a system with one additional defect (particle or hole) are calculated, the difference between these two energies vanishes at the boundary of Mott insulator phase. Then the solution of the equation, the difference of the two energies be zero, with respect to chemical potential μ will give phase boundary at the particle sector which is shown by μ_p. In a similar manner, phase boundary of the hole sector, μ_h, can be obtained from the equation where the energy difference of the Mott phase from one additional hole state becomes zero. In the strong coupling expansion, energies of each of these three states (Mott state, additional particle state and additional hole state) are calculated perturbatively. This method has been used for systems with different dimensions[26, 27] and for a two dimensional system under magnetic field[39].

To perform strong coupling expansion, it is convenient to write the Hamiltonian Eq.(4.1), in the following form,

$$H = -\sum_{ij} \mathbf{T}_{ij} a_i^\dagger a_j + \frac{1}{2}\sum_i n_i(n_i - 1) - \mu \sum_i n_i \tag{4.18}$$

where U is taken to be 1 and $\mathbf{T}_{ij}$ is the hopping matrix, which is

$$\mathbf{T} = t \begin{bmatrix} A & B & 0 & \dots & 0 & B^\dagger \\ B^\dagger & A & B & 0 & \ddots & 0 \\ 0 & B^\dagger & A & B & \ddots & \vdots \\ \vdots & \vdots & \ddots & \ddots & \ddots & 0 \\ 0 & \dots & 0 & B^\dagger & A & B \\ B & 0 & \dots & 0 & B^\dagger & A \end{bmatrix}. \tag{4.19}$$

A and B are 2×2 matrices of the form

$$A = \begin{pmatrix} 0 & 1 \\ 1 & 0 \end{pmatrix} \qquad B = \begin{pmatrix} e^{-i\alpha} & 0 \\ 0 & e^{i\alpha} \end{pmatrix} \tag{4.20}$$

and α is the same parameter as before. It can be seen that, with the appropriate labeling of sites as in Fig.4.6, this Hamiltonian is identical to the Hamiltonian in Eq.(4.1) where the upper leg was distinguised from the lower one. This form of Hamiltonian makes it easier to do perturbative calculations by considering the hopping $\mathbf{T}_{ij}$ as a general matrix which is real and symmetric.

We have performed strong coupling perturbation up to second order in our calculations. The energies of Mott state E_M, additional particle state E_P and additional hole state E_H are found to be (up to second order)

$$\begin{aligned} E_M &= E_M^0 - 3Nt^2 n_0(n_0+1) \\ E_P &= E_P^0 - (n_0+1)\lambda_{\mathbf{T}} - 3Nt^2 n_0(n_0+1) - n_0(n_0+1)\lambda_{\mathbf{T}}^2 + \frac{3}{2} n_0(5n_0+4)t^2 \\ E_H &= E_H^0 - n_0\lambda_{\mathbf{T}} - 3Nt^2 n_0(n_0+1) - n_0(n_0+1)\lambda_{\mathbf{T}}^2 + \frac{3}{2}(n_0+1)(5n_0+1)t^2 \end{aligned} \tag{4.21}$$

where $\lambda_{\mathbf{T}}$ is the lowest eigenvalue of the hopping matrix $\mathbf{T}$ and N is the number of lattice sites which is always even in the two leg ladder. Zeroth order energies are $E_M^0 = N(n_0(n_0-1)/2 - \mu n_0)$, $E_P^0 = E_M^0 + n_0 - \mu$ and $E_H^0 = E_M^0 - (n_0-1) + \mu$. A warning comes from first order corrections to E_P and E_H. Ground states of these two systems (one additional hole-particle) are N-fold degenerate. In the first order, these degeneracies do not split if the magnetic field is above the critical field α_c, which is expected because single particle solution give two degenerate energies above α_c as shown in Fig.4.6. On the other hand, matrix elements of the perturbation, the hopping term, among those two degenerate kets do not

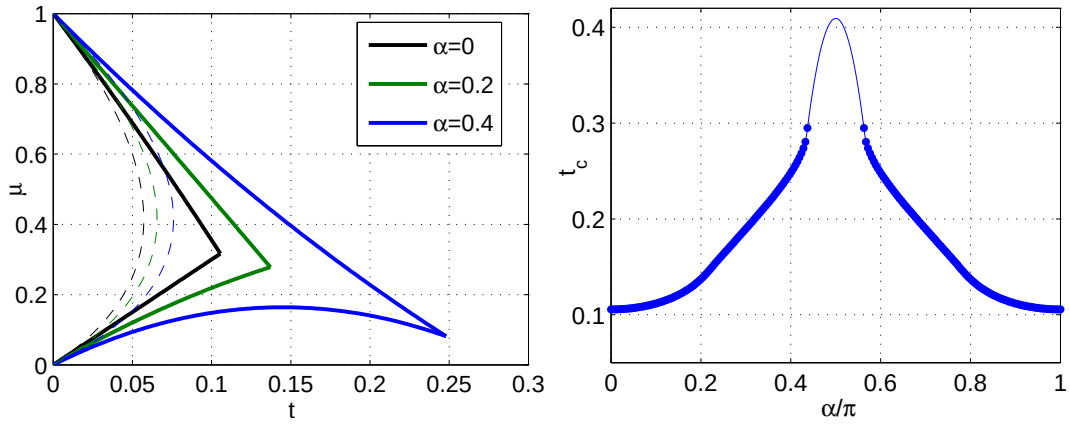

Figure 4.7: Phase diagram of two leg ladder, shown on the left, from strong coupling perturbation theory for magnetic fields $\alpha = 0$, $\alpha = 0.2$ and $\alpha = 0.4$ compared with the results of meanfield calculation (dotted thin lines). Above $\alpha = 0.43$ lines of μ_P and μ_H does not cross and higher oder perturbation is required. On the left the tip of the Mott region is shown as a function of field. Thin line after $\alpha = 0.43$ is spline interpolant.

have any off-diagonal elements. This enables us to apply standart second order perturbation safely as if the degeneracy is splitted in the first order[46]. Solving the equations $E_P - E_M = 0$ and $E_M - E_H = 0$ for the chemical potentials μ separately, the phase boundary of the particle and hole sector are obtained as,

$$\begin{aligned} \mu_P &= n_0 - (n_0+1)\lambda_{\mathbf{T}} - n_0(n_0+1)\lambda_{\mathbf{T}}^2 + \frac{3}{2}n_0(5n_0+4)t^2 \\ \mu_H &= (n_0-1) + n_0\lambda_{\mathbf{T}} + n_0(n_0+1)\lambda_{\mathbf{T}}^2 - \frac{3}{2}(n_0+1)(5n_0+1)t^2. \end{aligned} \tag{4.22}$$

Dependence of this form to the magnetic field comes indirectly from the eigenvalue $\lambda_{\mathbf{T}}$. To get a direct dependence on the field, higher order terms are required. An interesting observation is that our results are similar to the results of Ref.[39] up to second order if the number of nearest neighbors is taken 3, i.e $z = 3$. However this is not guaranteed for higher order expansions since the flux attained should be considered by additional particles and holes (see [26, 39] for details). The eigenvalue spectrum of the $\mathbf{T}$ matrix is already shown in Fig.4.2. Dependence of the minimum eigenvalue to the magnetic field is the dotted blue line in that figure. It is seen that the spectrum has no cusp unlike the results in two dimension[39].

Results of strong coupling expansion in 1D are shown to be in very good agreement with the numerically exact solutions[56, 57]. Thus, though we make perturbation up to only second order, they are expected to be reliable for our quasi-one dimensional system. In Fig.4.7 we have shown the results of our calculation. It can be seen that, increase of the magnetic field, increases the Mott insulating region. After some value of the magnetic field, reenterent behavior to the Mott phase appears, as it is seen for $\alpha = 0.4$ on the left panel. After about the point $\alpha = 0.43$ curves of particle and hole sector intersects at such a large value of magnetic field that the second order perturbation fails to obtain it and the two curves in Eq.(4.22) do not cross each other. However, apart from the cusplike dip that BKT transition takes place, the results are expected to be trustable. We have shown the change of critical hopping strength that BKT transition occurs as a function of magnetic field on the right panel. Above the point where two curves do not cross any more, a spline interpolation is done in that figure. In Fig.4.7, we have also shown the related sector from the results of meanfield calculation with dotted thin line. It is seen that mean field results can hardly describe the system properly. Besides, mean field theory is already expected to be poor for one dimensional systems as we have pointed out. A final remark is that, for strong magnetic field $\alpha_c > 0.4$ the phase diagram takes the shape of the one dimensional case found in [56]. The reenterent phase behavior found in one dimensional system appears with the increase of magnetic field for two leg ladder. This reenterent behavior was not previously seen in the results of strong coupling perturbation neither in one two and three dimensions nor in two dimensional lattice under magnetic field (in [26, 27, 39] perturbation was carried out up to third order). Existence of this reentrant phase is reliable since our system is essentially one dimensional where strong coupling approach performs its best.

4.5 DMRG Calculations

Density Matrix Renormalization Group (DMRG) theory has proven to provide numerically exact solutions of one dimensional lattice systems[40, 41]. DMRG

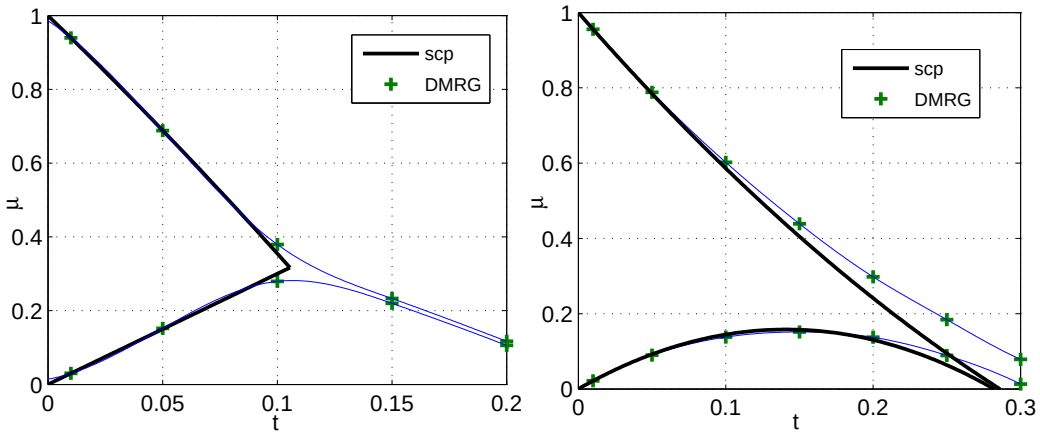

Figure 4.8: Phase diagram of two leg Bose Hubbard ladder for $\alpha = 0$ on the left and $\alpha = 0.45$ on the right. For comparison strong coupling results are also shown.

has been applied to one dimensional Bose Hubbard model as we have shown in Chapter 3. As a result, exact shape of phase diagram is obtained with/without nearest neighbor interaction[56, 57], existence of BKT transition is shown[58, 60] and correct phase diagram of disordered model is obtained[63]. This method is the most reliable approach for a one dimensional system regardless of the interaction strength for any correlated states. In this section, we will use DMRG to study the two leg Bose Hubbard ladder under magnetic field.

The details of the method was explained in Chapter 3. The basic idea can be summarized as follows. Starting from a size that can be diagonalized exactly, enlarge the system and sweep out the least relevant states by using the reduced density matrices until the desired system size is reached. Then employ the sweeping procedure which increases the accuracy up to machine precision. Recently, DMRG has been applied to two leg Bose Hubbard ladder but with different concerns[61]. We will use the similar method with [61], namely rung by rung enlargement. Different from this reference, we use the recently developed single site enlargement method[64].

Calculation of the Mott phase boundary via DMRG is similar to strong coupling perturbation method. One needs energies of Mott phase together with the

additional particle and hole states to find the Mott insulator boundary. Thus, the energies of particle and hole states are calculated as additional target states in DMRG implementation[56]. Generally some limiting cases that are exactly solvable are used to check the DMRG code. On the other hand, we have already obtained the strong coupling expansion results for the system. There must be an agreement between the two methods, especially for small hopping strength since we make perturbation only up to second order. In Fig.4.8, one can see the good agreement between the strong coupling result and DMRG. For larger values of hopping, the strong coupling expansion fails to capture the exact behavior. Another point is the existence of reentrant phase even for zero magnetic field, which is not seen by strong coupling. On the left panel we show the similar phase for $\alpha = 0.45$. Note that the strong coupling calculations give relatively poor results above $t \approx 0.2$ so that necessity of higher order terms becomes apparent. One thing to be noted is that the tip of the Mott insulator region requires a special treatment with DMRG. The two branches coming from particle and hole sector intersect in the thermodynamic limit. However, DMRG takes finite systems far from thermodynamic limit. There are several approaches (like consideration of correlation length and extrapolation to Luttinger liquid correlation function in [56]) to remedy this situation which we don't use because the tip of the lobe is not our main concern (see Chapter 3).

4.6 Evidence of Strongly Correlated Phases

Up to now, we have performed various analytical calculations that can only work around the Mott insulator phase. Theoretical approaches are quite limited for the Bose Hubbard model under magnetic field, particularly for strong fields. This is due to technical difficulties that stem from the strong correlations and high number of degeneracies. Both strong coupling and mean field approaches work on the region where those correlations are weak. On the other hand, the wealth of the system lies underneath these ignored identities. Thus, the characterization of the two dimensional Bose Hubbard model under strong magnetic field is very important which is a popular research area. There has been several proposals

that try the connect these strongly correlated states either with the formation of vortex lattice or with the incompressible quantum liquids found in quantum Hall effect. Difficulty of the solution of the theoretical model makes it a hard task to show the exact nature of the system. What can be done at best is an exact diagonalization study of a small sized system with a few number of particles. But these solutions are far from the thermodynamic limit and it has been found that for strong magnetic fields the system does not resemble to be in some known incompressible liquid phase[32, 37].

Strong coupling as well as mean field theory can predict quantum states near Mott insulator phase as we have shown. They are valid when the total number of particles is equal to the total number of lattice sites. On the other edge, Gross Pitaevskii approximation assumes a uniform gas spread over the lattice to reveal the dynamics of the system. Compared to these theoretical approaches, DMRG gives a very wide range of applicability regardless of the particle number, strength of the field and the interaction. One can calculate the ground state of the system with any finite lattice size and any number of particles for all values of the magnetic field and the interaction strength (as long as the eigenvalue spectrum of the density matrix decays exponentially). The main drawback of DMRG is that it can only be applied to one dimensional systems. The algorithm is difficult to implement even for a few legged one dimensional systems. Another point is the fact that DMRG works for finite sized systems which may be particularly important for the properties in the thermodynamic limit. In this section we will use DMRG to study the two leg Bose Hubbard model under magnetic field out of the Mott insulator region.

We make DMRG calculations for hard core bosons in infinite U limit. Providing an easier implementation of the algorithm which also works fast, this limit is particularly important for experimental realizations. Because the gaps are expected to be more prominent with strong interactions. With this approximation each site is allowed to be empty or have only one boson so that maximum occupation number $n_{max} = 1$ and the term with the onsite interaction in the Hamiltonian is removed. In this approximation, Bose Hubbard model is expected to be mapped to spin-XXZ model, where ground state is at half filling[51]. We found

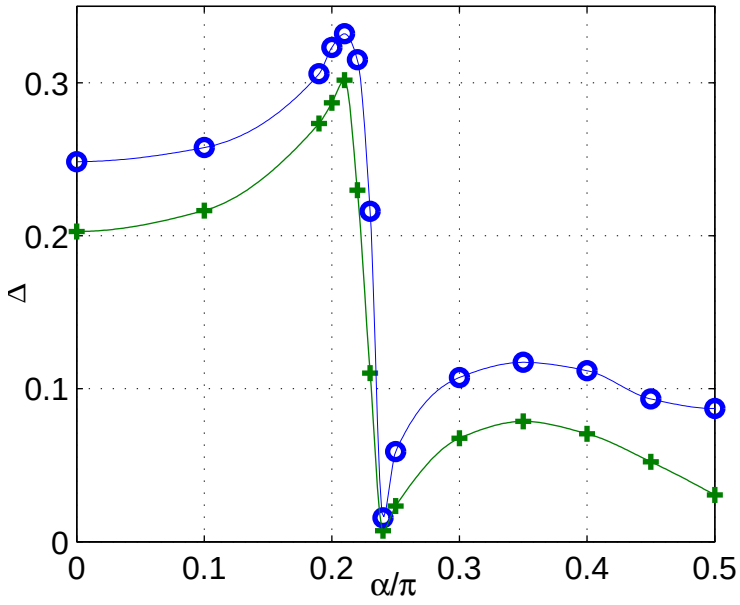

Figure 4.9: Gap between ground state and two excited states for different magnetic field. The gap between first excited state $E^1 - E^0$ is shown by green '+', whereas the one for $E^2 - E^0$ is shown by blue '$\circ$'. Thin lines are spline interpolation to data points. It is seen that around $\alpha_c = 0.21$ spectrum has a jump to a completely different behavior.

that our system has a ground state at half filling not only for $\alpha = 0$ but also for nonzero α. In two distinct limits; all sites are empty and all sites are filled, ground state energy is zero and minimum of the energy is always at half filling which is in the middle of these two limits.

We obtain energies for different values of magnetic field, on the half filling particle sector of the superblock Hamiltonian. The energy gap between the ground state and first two excited states is obtained and shown in Fig.4.9. From the figure, it can be seen that spectrum of the three lowest lying states changes abruptly to a different pattern at $\alpha_c = 0.21$. This plot is symmetric around $\alpha = 0.5$ so we only show one half. The critical value found here is perfectly consistent with the one found in single particle solution, which were equal to 0.2148 or 0.7852. Note that spectrum is not smooth at $\alpha = 0.5$ but has a cusp.

To get the energies at various fillings, we use the route proposed by Ramanan

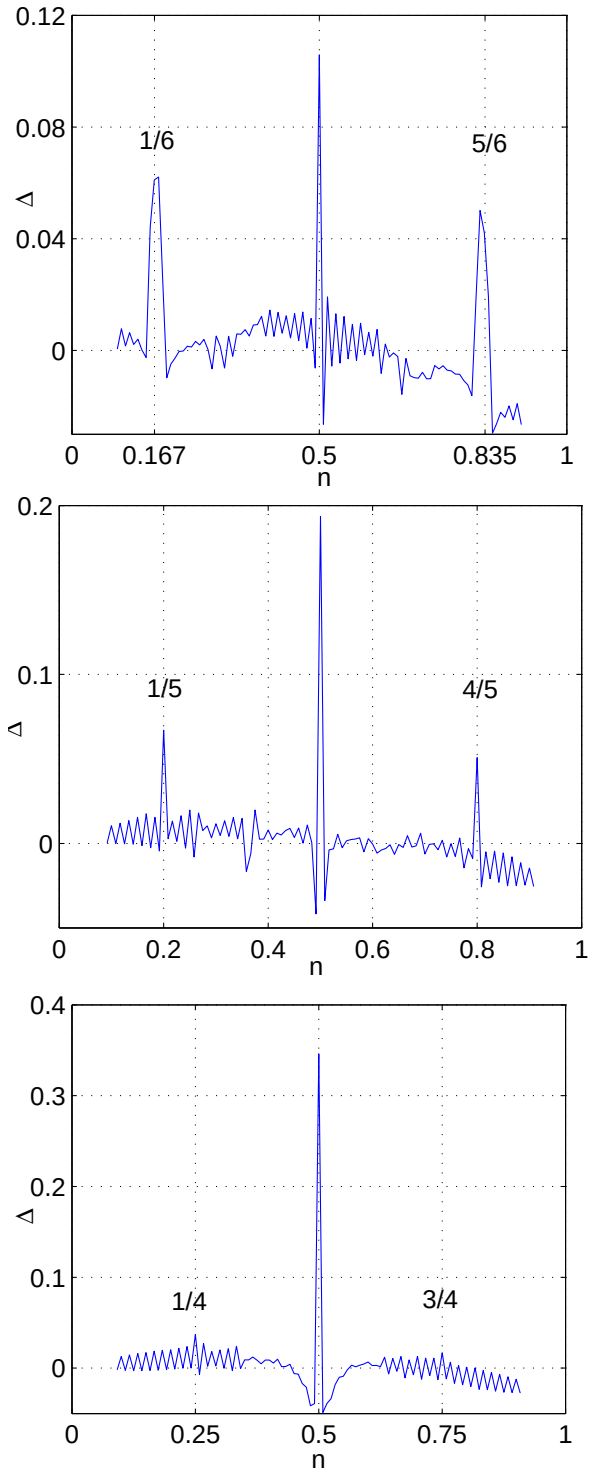

Figure 4.10: Energy gap defined in Eq.4.23 as a function of particle density for $\alpha = 1/3$ in the first figure, $2/5$ in the second and $1/2$ in the third respectively. For each value of α, a different peak is seen in the energy gap where the peaks are symmetric around 0.5. Apart from the dominant peaks at $1/5$, $1/6$ for $\alpha = 1/3$, $1/5$, $4/5$ for $\alpha = 2/5$ and $1/4$, $3/4$ $\alpha = 1/2$ and the persistent peak at $1/2$, there seem to be fluctuating non zero gap value for other fillings.

Table 4.1: Value of the filling factor defined in Eq.4.24 for different magnetic fields shown in Fig.4.10

α	n_1	ν_1	n_2	ν_2	n_3	ν_3
1/3	1/6	1/2	5/6	3/2	5/6	5/2
2/5	1/5	1/2	4/5	5/4	4/5	2
1/2	1/4	1/2	3/4	1	3/4	3/2

et al.[60] for a system of length $L = 60$ that has $2 \times L = 120$ sites. Beginning from $L = 4$ and total number of particles $N = 4$ (since we know minimum energy is at half filling for infinite U), we increase both the lattice length and the number of particles up to where the total number of particles is, lets say, $N = 10$. After that, the lattice length is increased while total number of particles held fixed at 10. Whenever lattice length reaches the desired length, $L = 60$, finite system sweeps are used to get better energy. Next the system size is held fixed while particle number is increased, by doing 5 sweeps for each particle number. Total number of particles is increased up to $N = 110$. At the end, energies of systems from $N = 10$ to $N = 110$ particles placed on $2 \times L = 120$ sites are obtained. Ramanan *et al.* obtained the plateaus in the chemical potential versus density plots and corresponding compressibilities by using this method. After that, the gap formula defined by Cooper *et al.*[65] is used which has the form

$$\Delta = N \left[\frac{E(N+1)}{N+1} + \frac{E(N-1)}{N-1} - 2\frac{E(N)}{N} \right] \tag{4.23}$$

which minimizes the finite size effects. This gap is shown for various values of magnetic field in Fig.4.10. It is seen that the gap oscillates between zero and nonzero values for low densities and becomes negative towards interger filling. Apart from that, there are three dominant peaks one is always at 1/2 and the other two change with different α. Magnitude of these changing peaks are also seen to be getting smaller and smaller as the field approaches 1/2. It is interesting to compare these peaks by defining the filling factor[66],

$$\nu = \frac{n}{f} \tag{4.24}$$

where n is particle density and f is vortex density defined as the phase attained around a unit cell divided by 2π. In our model, it can be shown that $2\pi f = 2\alpha$ so

that $f = \alpha/\pi$. In Table 4.1, we have shown the values of filling factor by looking at the peaks in Fig.4.10. One can see that various fillings are obtained as 1/2, 1, 5/4, 3/2, 5/2.

4.7 Conclusion

We have studied on the two leg Bose Hubbard ladder exposed to a strong magnetic field within various theoretical approaches and implemented DMRG to study the exact behavior of the system. It is found that system has two different behaviors above and below the critical magnetic field. The shape of the Mott insulator region is obtained within three different methods; variational meanfield theory, strong coupling perturbation and DMRG. It is found that the shape of the lobe is very consistent within DMRG and strong coupling whereas the results of the meanfield theory is relatively poor. This was already expected because mean field theory ignores the strong correlations that are particularly important for low dimensional systems. Apart from the determination of the Mott lobes, the system is found to display novel physical properties from the results of single particle spectrum and Gross Pitaevskii approximation. We believe that this toy model serves as an important tool for understanding the general properties of the rotating optical lattices and the theoretical methods that are used most frequently. In the last part of the chapter, we have worked on the characterization of strongly correlated phases in the hard core limit. The system is found to display incompressible liquid phases at various fillings depending on the field strength where these states are completely different from the incompressible Mott insulator state. Our work on the system for soft bosons (that is, different from the infinite U limit) is in progress. This system is believed to be very rich for the exploration of exotic quantum phases.

Bibliography

[1] F Dalfovo, S Giorgini, LP Pitaevskii, and S Stringari. Theory of Bose-Einstein condensation in trapped gases. *Reviews of Modern Physics*, 71(3):463–512, Apr 1999.

[2] Kerson Huang. *Statistical mechanics*. Wiley, 1987.

[3] Wolfgang Ketterle. Nobel lecture: When atoms behave as waves: Bose-einstein condensation and the atom laser. *Reviews of Modern Physics*, 74(4):1131+, November 2002.

[4] E. A. Cornell and C. E. Wieman. Nobel lecture: Bose-einstein condensation in a dilute gas, the first 70 years and some recent experiments. *Rev. Mod. Phys.*, 74(3):875–893, Aug 2002.

[5] AJ Leggett. Bose-Einstein condensation in the alkali gases: Some fundamental concepts. *Reviews of Modern Physics*, 73(2):307–356, Apr 2001.

[6] V. I. Yukalov. Cold bosons in optical lattices. *Laser Physics*, 19(1):1–110, Jan 2009.

[7] A. J. Leggett. *Quantum liquids : Bose condensation and Cooper pairing in condensed-matter systems*. Oxford University Press, 2008.

[8] H. Smith C. J. Pethick. *Bose-Einstein condensates in dilute atomic gases*. Cambridge University Press, 2002.

[9] Alexander L. Fetter. Rotating trapped bose-einstein condensates. *Reviews of Modern Physics*, 81(2):647, 2009.

[10] James F. Annet. *Superconductivity, Superfluids and Condensates*. Oxford University Press, 2004.

[11] A. L. Fetter and J. D. Walecka. *Quantum Theory of Many Particle Systems*. Dover Publications, 2003.

[12] TL Ho. Bose-Einstein condensates with large number of vortices. *Physical Review Letters*, 87(6), Aug 6 2001.

[13] S Stock, B Battelier, V Bretin, Z Hadzibabic, and J Dalibard. Bose-Einstein condensates in fast rotation. *Laser Physics Letters*, 2(6):275–284, Jun 2005.

[14] V. Schweikhard, I. Coddington, P. Engels, V. P. Mogendorff, and E. A. Cornell. Rapidly rotating bose-einstein condensates in and near the lowest landau level. *Phys. Rev. Lett.*, 92(4):040404, Jan 2004.

[15] Vincent Bretin, Sabine Stock, Yannick Seurin, and Jean Dalibard. Fast rotation of a bose-einstein condensate. *Phys. Rev. Lett.*, 92(5):050403, Feb 2004.

[16] Rajiv Bhat, M. Krämer, J. Cooper, and M. J. Holland. Hall effects in bose-einstein condensates in a rotating optical lattice. *Physical Review A (Atomic, Molecular, and Optical Physics)*, 76(4):043601, 2007.

[17] S. Tung, V. Schweikhard, and E. A. Cornell. Observation of vortex pinning in bose-einstein condensates. *Physical Review Letters*, 97(24):240402, 2006.

[18] Matthew P. A. Fisher, Peter B. Weichman, G. Grinstein, and Daniel S. Fisher. Boson localization and the superfluid-insulator transition. *Phys. Rev. B*, 40(1):546–570, Jul 1989.

[19] D Jaksch, C Bruder, JI Cirac, CW Gardiner, and P Zoller. Cold bosonic atoms in optical lattices. *Physical Review Letters*, 81(15):3108–3111, Oct 12 1998.

[20] D van Oosten, P van der Straten, and HTC Stoof. Quantum phases in an optical lattice. *Physical Review A*, 63(5), May 2001.

[21] M Greiner, O Mandel, T Esslinger, TW Hansch, and I Bloch. Quantum phase transition from a superfluid to a Mott insulator in a gas of ultracold atoms. *Nature*, 415(6867):39–44, Jan 3 2002.

[22] I Bloch. Ultracold quantum gases in optical lattices. *Nature Physics*, 1(1):23–30, Oct 2005.

[23] Immanuel Bloch, Jean Dalibard, and Wilhelm Zwerger. Many-body physics with ultracold gases. *Reviews of Modern Physics*, 80(3):885, 2008.

[24] C Bruder, R Fazio, and G Schon. The Bose-Hubbard model: from Josephson junction arrays to optical lattices. *Annalen Der Physik*, 14(9-10):566–577, Sep-Oct 2005.

[25] K Sheshadri, HR Krishnamurthy, R Pandit, and TV Ramakrishnan. Superfluid and Insulating Phases in an Interacting-Boson Model - Mean-Field Theory and the RPA. *Europhysics Letters*, 22(4):257–263, May 1 1993.

[26] JK Freericks and H Monien. Phase-Diagram of the Bose-Hubbard Model. *Europhysics Letters*, 26(7):545–550, Jun 1 1994.

[27] J. K. Freericks and H. Monien. Strong-coupling expansions for the pure and disordered bose-hubbard model. *Phys. Rev. B*, 53(5):2691–2700, Feb 1996.

[28] M. Iskin and J. K. Freericks. Strong-coupling perturbation theory for the extended Bose-Hubbard model. *Physical Review A*, 79(5), May 2009.

[29] Douglas R. Hofstadter. Energy levels and wave functions of bloch electrons in rational and irrational magnetic fields. *Phys. Rev. B*, 14(6):2239–2249, Sep 1976.

[30] JG Analytis, SJ Blundell, and A Ardavan. Landau levels, molecular orbitals, and the Hofstadter butterfly in finite systems. *American Journal of Physics*, 72(5):613–618, May 2004.

[31] Susanne Viefers. Quantum hall physics in rotating Bose-Einstein condensates. *Journal of Physics-Condensed Matter*, 20(12), Mar 26 2008.

[32] R Bhat, MJ Holland, and LD Carr. Bose-Einstein condensates in rotating lattices. *Physical Review Letters*, 96(6), FEB 17 2006.

[33] RN Palmer and D Jaksch. High-field fractional quantum Hall effect in optical lattices. *Physical Review Letters*, 96(18), May 12 2006.

[34] Rajiv Bhat, B. M. Peden, B. T. Seaman, M. Kramer, L. D. Carr, and M. J. Holland. Quantized vortex states of strongly interacting bosons in a rotating optical lattice. *Physical Review A*, 74(6), Dec 2006.

[35] Rajiv Bhat, M. Kraemer, J. Cooper, and M. J. Holland. Hall effects in Bose-Einstein condensates in a rotating optical lattice. *Physical Review A*, 76(4), Oct 2007.

[36] M. Hafezi, A. S. Sorensen, E. Demler, and M. D. Lukin. Fractional quantum Hall effect in optical lattices. *Physical Review A*, 76(2), Aug 2007.

[37] Gunnar Moller and Nigel R. Cooper. Composite fermion theory for bosonic atoms in optical lattices, 2009.

[38] R. O. Umucalilar and M. O. Oktel. Phase boundary of the boson Mott insulator in a rotating optical lattice. *Physical Review A*, 76(5), Nov 2007.

[39] M. Niemeyer, J. K. Freericks, and H. Monien. Strong-coupling perturbation theory for the two-dimensional bose-hubbard model in a magnetic field. *Phys. Rev. B*, 60(4):2357–2362, Jul 1999.

[40] Steven R. White. Density matrix formulation for quantum renormalization groups. *Phys. Rev. Lett.*, 69(19):2863–2866, Nov 1992.

[41] Steven R. White. Density-matrix algorithms for quantum renormalization groups. *Phys. Rev. B*, 48(14):10345–10356, Oct 1993.

[42] Steven R. White and David A. Huse. Numerical renormalization-group study of low-lying eigenstates of the antiferromagnetic s=1 heisenberg chain. *Phys. Rev. B*, 48(6):3844–3852, Aug 1993.

[43] KG Wilson. The renormalization and critical phenomena. *Reviews Of Modern Physics*, 55(3):583–600, 1983.

[44] U. Schollwöck. The density-matrix renormalization group. *Rev. Mod. Phys.*, 77(1):259–315, Apr 2005.

[45] N Shibata. Application of the density matrix renormalization group method to finite temperatures and two-dimensional systems. *Journal of Physics A-Mathematical and General*, 36(37):R381–R410, Sep 19 2003.

[46] J.J. Sakurai. *Modern Quantum Mechanics*. Addison-Wesley, revised edition, 1994.

[47] Richard Phillips Feynman. *Statistical mechanics; a set of lectures / Ed. by Jacob Shaham.* Addison-Wesley, 1972.

[48] M. Kaulke I. Peschel, X. Wang and K. Hallberg (Eds.). *Density-matrix renormalization: a new numerical method in physics : lectures of a seminar and workshop held at the Max-Planck-Institut fr Physik Komplexer Systeme, Dresden, Germany, August 24th to September 18th, 1998*. Springer Verlag, 1999.

[49] SR White and RM NOACK. Real space quantum-renormalization groups. *Physical Review Letters*, 68(24):3487–3490, Jun 15 1992.

[50] RM Noack and SR Manmana. Diagonalization- and numerical renormalization-group-based methods for interacting quantum systems. In Avella, A and Mancini, F, editor, *Lectures on the Physics of Highly Correlated Electron Systems IX*, volume 789 of *AIP Conference Proceedings*, pages 93–163, 2005. 9th Training Course in the Physics of Correlated Electron Systems and High-Tc Superconductors, Salerno, ITALY, OCT 04-15, 2004.

[51] I Affleck. Quantum spin chains and the Haldane gap. *Journal of Physics-Condensed Matter*, 1(19):3047–3072, May 15 1989.

[52] Elliott Lieb, Theodore Schultz, and Daniel Mattis. Two soluble models of an antiferromagnetic chain. *Annals of Physics*, 16(3):407–466, December 1961.

[53] AL Malvezzi. An introduction to numerical methods in low-dimensional quantum systems. *Brazilian Journal of Physics*, 33(1):55–72, Mar 2003.

[54] FDM Haldane. Continuum dynamics of the 10D Heisenberg anti-ferromagnet - identification with the O(3) non-linear sigma-model. *Physics Letters A*, 93(9):464–468, 1983.

[55] R. M. Noack, S. R. White, and D. J. Scalapino. Correlations in a two-chain hubbard model. *Phys. Rev. Lett.*, 73(6):882–885, Aug 1994.

[56] TD Kuhner, SR White, and H Monien. One-dimensional Bose-Hubbard model with nearest-neighbor interaction. *Physical Review B*, 61(18):12474–12489, May 1 2000.

[57] TD Kuhner and H Monien. Phases of the one-dimensional Bose-Hubbard model. *Physical Review B*, 58(22):14741–14744, Dec 1 1998.

[58] RV Pai, R Pandit, HR Krishnamurthy, and S Ramasesha. One-dimensional disordered bosonic Hubbard model: A density-matrix renormalization group study. *Physical Review Letters*, 76(16):2937–2940, APR 15 1996.

[59] RV Pai and R Pandit. Superfluid, Mott-insulator, and mass-density-wave phases in the one-dimensional extended Bose-Hubbard model. *Physical Review B*, 71(10), Mar 2005.

[60] S. Ramanan, Tapan Mishra, Meetu Sethi Luthra, Ramesh V. Pai, and B. P. Das. Signatures of the superfluid-to-Mott-insulator transition in cold bosonic atoms in a one-dimensional optical lattice. *Physical Review A*, 79(1), Jan 2009.

[61] Meetu Sethi Luthra, Tapan Mishra, Ramesh V. Pai, and B. P. Das. Phase diagram of a bosonic ladder with two coupled chains. *Physical Review B*, 78(16), Oct 2008.

[62] L. D. Landau and E. M. Lifshitz. *Statistical physics: Vol.2.* Pergamon Press, 1980.

[63] S Rapsch, U Schollwock, and W Zwerger. Density matrix renormalization group for disordered bosons in one dimension. *Europhysics Letters*, 46(5):559–564, Jun 1 1999.

[64] Steven R. White. Density matrix renormalization group algorithms with a single center site. *Phys. Rev. B*, 72(18):180403, Nov 2005.

[65] N. R. Cooper, N. K. Wilkin, and J. M. F. Gunn. Quantum phases of vortices in rotating bose-einstein condensates. *Phys. Rev. Lett.*, 87(12):120405, Aug 2001.

[66] N. R. Cooper. Rapidly rotating atomic gases. *Advances In Physics*, 57(6):539–616, 2008.